NASA TECHNICAL NOTE

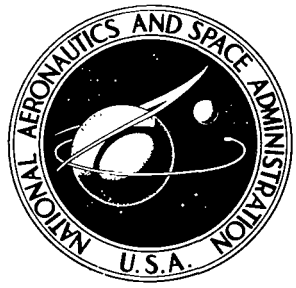

NASA TN D-6918

DESIGN AND EVALUATION OF AN OXIDANT-FUEL-RATIO-ZONED ROCKET INJECTOR FOR HIGH PERFORMANCE AND ABLATIVE ENGINE COMPATIBILITY

by Jerry M. Winter, Albert J. Pavli, and Arthur M. Shinn, Jr.

Lewis Research Center
Cleveland, Ohio 44135

NATIONAL AERONAUTICS AND SPACE ADMINISTRATION • WASHINGTON, D. C. • AUGUST 1972

1. Report No.	2. Government Accession No.	3. Recipient's Catalog No.
NASA TN D-6918		

4. Title and Subtitle: DESIGN AND EVALUATION OF AN OXIDANT-FUEL-RATIO-ZONED ROCKET INJECTOR FOR HIGH PERFORMANCE AND ABLATIVE ENGINE COMPATIBILITY

5. Report Date: August 1972

6. Performing Organization Code:

7. Author(s): Jerry M. Winter, Albert J. Pavli, and Arthur M. Shinn, Jr.

8. Performing Organization Report No.: E-6945

10. Work Unit No.: 113-31

9. Performing Organization Name and Address:
Lewis Research Center
National Aeronautics and Space Administration
Cleveland, Ohio 44135

11. Contract or Grant No.:

13. Type of Report and Period Covered: Technical Note

12. Sponsoring Agency Name and Address:
National Aeronautics and Space Administration
Washington, D.C. 20546

14. Sponsoring Agency Code:

15. Supplementary Notes:

16. Abstract

The program goal was to design and demonstrate a method for temperature control of the combustion gases in the peripheral zone of a rocket combustor which would reduce ablative throat erosion, prevent melting of zirconia throat inserts, and maintain high combustion performance. Included are techniques for analyzing and predicting zoned injector performance, as well as the philosophy and method for accomplishing an optimum compromise between high performance and reduced effective gas temperature. The experimental work was done with a 4450-N (1000-lbf) rocket engine which used as propellants N_2O_4 and a blend of 50-percent N_2H_4 and 50-percent UDMH at 690-kN/m^2 (100-psia) chamber pressure and an overall O/F of 2.0. The method selected to provide temperature control was to use 30 percent of the propellant to form a peripheral zone of combustion gases at an O/F of 1.31 and 2700 K (4861° R). The remaining 70 percent of the propellant in the core was at an O/F of 2.45 to keep the overall O/F at 2.0. Zoned combustion produced a calculated temperature decrease from the unzoned case of 275 K (495° R) with a vacuum specific impulse decrease of 72.6 N-sec/kg (7.4 lbf-sec/lbm), or 2.2 percent of theoretical kinetic. This temperature decrease lowered the ablative throat erosion rate from 0.013 cm/sec (0.0052 in./sec) to 0.0076 cm/sec (0.003 in./sec) and prevented melting of zirconia throat inserts.

17. Key Words (Suggested by Author(s)): O/F zoning; Combustion performance; Rocket engine; Earth storable propellants; Ablative compatibility; Effective gas temperature

18. Distribution Statement: Unclassified - unlimited

19. Security Classif. (of this report)	20. Security Classif. (of this page)	21. No. of Pages	22. Price*
Unclassified	Unclassified	58	$3.00

* For sale by the National Technical Information Service, Springfield, Virginia 22151

DESIGN AND EVALUATION OF AN OXIDANT-FUEL-RATIO-ZONED ROCKET INJECTOR FOR HIGH PERFORMANCE AND ABLATIVE ENGINE COMPATIBILITY

by Jerry M. Winter, Albert J. Pavli, and Arthur M. Shinn, Jr.

Lewis Research Center

SUMMARY

A method was demonstrated whereby temperature control of the combustion gases in the peripheral zone of a rocket combustor was used to provide ablative and throat insert durability. The goal of the program was to arrive at a zone temperature of combustion which was low enough to prevent melting of a zirconia throat insert while maintaining specific impulse performance equivalent to at least 3016 N-sec/kg (307.5 lbf-sec/lbm) at an expansion area ratio of 60. This goal was met with a peripheral combustion gas temperature of 2700 K (4861° R) and a specific impulse value of 3026 N-sec/kg (308.6 lbf-sec/lbm). The experimental work was done with a 4450-N (1000-lbf) rocket engine which used nitrogen tetroxide and a 50-percent blend of hydrazine with unsymmetrical dimethyl hydrazine propellants at 690-kN/m^2 (100-psia) chamber pressure and an oxidant-to-fuel mixture ratio (O/F) of 2.0.

Performance losses associated with various temperature control methods were both measured and calculated. The method selected to prevent insert melting was to use 30 percent of the propellant mass flow to form an outer peripheral zone of combustion gases at an O/F of 1.31. The remaining 70 percent of the propellant mass flow in the center core was set at an O/F of 2.45 in order to keep the overall O/F at 2.0. This technique produced a calculated temperature decrease of 275 K (495° R) in the peripheral zone, with an attendant specific impulse decrease of 72.6 N-sec/kg (7.4 lbf-sec/lbm). A direct correlation between ablative erosion and peripheral-zone combustion temperature was also shown.

An optimum design would set the core O/F at the maximum performance for the particular injector in use. The zone O/F would be set to provide the desired temperature, and the amount of mass flow in the outer zone would be minimized. For the 70-percent core - 30-percent zone mass split used with injector 2, a core O/F of 1.8 and a zone O/F of 1.31 would give the desired zone temperature at an overall O/F of 1.65. A performance gain of 52.0 N-sec/kg (5.3 lbf-sec/lbm) over the method used herein would then be realized.

INTRODUCTION

Development of ablative rocket engines using earth-storable propellants requires not only good injector design to provide high combustion efficiency, but also suitable materials for the nozzle throat to maintain dimensional stability and thus high specific impulse over the life of the mission. Propellants of particular interest were nitrogen tetroxide and a 50-percent blend of unsymmetrical dimethyl hydrazine with hydrazine (as used on contemporary spacecraft) at a chamber pressure of 690 kN/m^2 (100 psia). Previous reports in this effort have dealt with ablative (ref. 1) and insert materials (ref. 2) to provide the required dimensional stability for 3.05-centimeter (1.2-in.) throat diameters. The purpose of the work reported in reference 3 was to develop 7.62-centimeter (3.0-in.) diameter hard throat inserts for application to long-term (700 sec total) duty cycles with restart capability as well as steady-state operation (300 sec continuous). In the course of testing these 7.62-centimeter (3.0-in.) diameter throat inserts, it was found necessary to modify the combustion environment to provide the desired lifetime since better materials were not available. In this report are discussed injector design changes intended to provide a cooler combustion temperature environment near the chamber wall while maintaining an engine performance level of 95-percent theoretical equilibrium characteristic exhaust velocity C^*_{theo}. This is equivalent to a vacuum specific impulse of 3016 N-sec/kg (307.5 lbf-sec/lbm) at an expansion area ratio of 60.

The present discussion details the procedure followed in terms of temperature, ablative compatibility, combustion performance, and vacuum specific impulse performance. While other work determined available performance for earth-storable propellants (ref. 4) and designed zoned injectors (refs. 5 and 6), the work herein includes correlation of performance with ablative erosion and measured combustion gas temperatures. Methods to improve upon the results are also suggested. The intention is to provide general guidelines for control of the temperature of the outer zone of combustion with as little loss in overall performance as possible.

The approach of the injector modification program was to achieve improved ablative and throat insert durability by decreasing the peripheral-zone combustion temperature of a high-performance injector. A design temperature range of 2660 to 2720 K (4800° to 4900° R) was selected because previous experience indicated this range would prevent zirconia insert melting found with the unmodified injector operating at a combustion temperature of 2980 K (5360° R). Lower temperatures would give more safety margin but might prevent achievement of the 95-percent C^*_{theo} performance goal.

The combustion temperature for earth-storable propellants was seen to be more sensitive to decreased oxidant-to-fuel mixture ratio (O/F) than to increased O/F. Hence, it was decided to lower the peripheral-zone combustion temperature by decreasing the O/F of the peripheral zone. It was decided to keep the overall O/F at 2.0 to

make the work more directly comparable to the previous work of references 1 and 2. This also maintains more favorable bulk density characteristics for contemporary spacecraft tankage but necessitates operating the injector core at O/F's higher than 2.0.

The report proceeds through injector design, modification for ablative-insert compatibility, and the effect upon delivered vacuum specific impulse. A section on suggestions to improve upon the results is included.

This report displays all values in the International System of Units (SI) as the primary system. U. S. customary units appear as a secondary system in parentheses after the SI values. The measurements and calculations for this work were done in U. S. customary units.

APPARATUS

Facility

Figure 1 shows the test facility. The flow system is illustrated schematically in figure 2. An engine was installed in the horizontal thrust stand. The nozzle exhausted to the atmosphere. The exhaust products were then collected and water scrubbed. The thrust stand was supported on precision-ground flexure plates to provide rigid restraint in all directions, except axial, with respect to the engine centerline. In the axial direction, the thrust stand was restrained entirely by the load cell, which was mounted in tension on spherical bearings. The load cell, a dual-bridge strain-gage transducer, was kept in tension by a preload spring of low spring constant to preclude the load on the load cell from ever becoming compressive.

To avoid any extraneous forces from propellant piping, the feedlines were either flex hoses or long lines entering at right angles to the thrust axis. The effects of the preload spring, the spring constant of the flexure plates, and the spring constant of the propellant piping on the operation of the thrust stand were accounted for by careful in-place calibration. The calibration was performed at regular intervals by pulling on the thrust stand in precise alinement with the engine centerline by means of a calibration load cell in series with a hydraulic cylinder. The calibration load cell was also a dual-bridge strain-gage transducer which was periodically calibrated by hanging precision deadweights from it.

Instrumentation

Chamber pressure measurements were made by using redundant strain-gage bridge

pressure transducers connected through a hole in the injector face. Both fuel and oxidant flow rates were measured by venturi and turbine meters in series. Iron constantan thermocouples were used to measure propellant temperatures. Open-bead tungsten/tungsten-rhenium thermocouples were used to measure combustion gas temperature at the rocket throat. The wire diameter was 0.051 centimeter (0.020 in.) and the bead diameter was 0.097 centimeter (0.038 in.). The beads were located at depths of 0.102, 0.254, 0.477, and 0.610 centimeter (0.040, 0.100, 0.180, and 0.240 in.) into the combustion gas stream. At each depth, three thermocouples were spaced 120° apart to provide good circumferential coverage. The heat-sink nozzle with thermocouples installed is illustrated in figure 3.

Data Recording and Processing

Electrical outputs of 50 channels were sampled at 2500 samples per second so that each output was recorded at 0.02-second intervals. Electrical signals were then digitized and recorded on magnetic tape. The data were converted to engineering quantities and the appropriate calculations were made by a digital computer. Selected sensor outputs were also recorded continuously on strip charts and an oscillograph for system monitoring and control room processing.

Thrust Chamber Assembly

Injectors. - Table I is a summary of the design values for all the injectors used in the program. The pattern and element detail of injectors 1, 2, 2A, 2B, and 2C are shown in figures 4, 5, and 6, respectively.

The basic injector designs were fuel-oxidant-fuel triplets similar to those used in previous programs with the same propellants (ref. 7). Triplet elements were originally selected because of their very good liquid atomization characteristics (ref. 8) and their ability to provide axial resultant momentum over a range of operating conditions. The use of uniform injector face coverage, oxidant hole sizes of 0.109-centimeter (0.043-in.) diameter or less, and oxidant-to-fuel velocity ratios of 0.6 and 0.7 had previously provided high combustion performance but not erosion-free ablative operation. The approach in those earlier studies was to maintain high performance and attempt to combat ablative throat erosion by the application of hard throat inserts.

Injector 1 (fig. 4) had the 61 triplet elements arranged radially to provide spray fans parallel to the wall for ablative compatibility. The elements were arranged in four circles about a center element in a circumferential spacing that was very nearly

TABLE I. - INJECTOR DESCRIPTION

Injector			Oxidant holes			Fuel holes			Design oxidant-to-fuel ratio, OF	Design velocity ratio, v_{ox}/v_f	Impingement		
Designation	Type	Pattern	Number	Diameter		Number	Diameter				Distance		Included angle between fuels, deg
				cm	in.		cm	in.			cm	in.	
1	Triplet (fuel on oxidant)	Circular (radial element)	61	0.109	0.043	122	0.053	0.021	2.00	0.60	1.421	0.560	40
2	Triplet (fuel on oxidant)	Mutually perpendicular grid	137	0.089	0.035	274	0.046	0.018	2.00	0.67	1.310	0.516	30
2A	Triplet (low O/F zone on outside)	Mutually perpendicular grid	101 36	0.089 .089	0.035 .035	202 72	0.046 .061	0.018 .024	2.55 1.21	0.96	1.310	0.516	30
2B	Triplet (low O/F zone on outside)	Mutually perpendicular grid with zone elements radial	101 30 6	0.089 .089 .089	0.035 .035 .035	202 60 12	0.046 .057 .061	0.018 .0225 .024	2.30 1.40	0.80	1.310	0.516	30
2C	Triplet and quadlet (low O/F zone on outside)	Mutually perpendicular grid with outer elements arranged three fuel holes and one oxidant hole	101 36	0.089 .089	0.035 .035	202 64 30 14	0.046 .041 .057 .061	0.018 .016 .0225 .024	2.45 1.31	0.86	1.310	0.516	30

the same as the radial spacing. This resulted in the elements being distributed uniformly across the whole area of the injector face. The arrangement of elements, as mentioned, was radial with the resultant spray fans parallel to the chamber wall and nearly parallel to adjacent spray fans. In view of experience with unlike doublet elements, it is likely that the distribution of propellants in a spray fan is not particularly uniform. The authors postulate a mirror image of two unlike doublets together producing fuel-rich zones on the sides of the spray fans and oxidant-rich zones on the ends of the spray fans. With a parallel fan arrangement, any intra-element reaction is discouraged, since spray fans would intersect with fuel-rich side onto fuel-rich side, and oxidant-rich end onto oxidant-rich end. The relation of this intra-element reaction was changed in the design of injector 2 (see fig. 5). This injector had triplet elements arranged in a grid pattern uniformly distributed over the entire area of the injector face. Fineness and uniformity of propellant distribution was improved over that of injector 1 by increasing the number of elements (137 instead of 61) and by orienting the elements mutually perpendicular to enhance intra-element reactions. The spray fans in injector 2 intersected a fuel-rich side onto an oxidant-rich end, and conversely. Modifications to injector 2 were evolved during the course of the program, based upon experimental results. Therefore, these modifications are described in the order in which the rationale for their design is discussed.

Thrust chambers. - The requirements of the program necessitated four different thrust chamber designs. First, a heat-sink thrust chamber (fig. 7) was used to provide engine performance data during short firings. A flame-sprayed zirconia coating provided thermal protection to the steel for firing durations as long as 7 seconds. A contraction ratio of 3 and a combined length from injector to throat of 47.17 centimeters (18.57 in.) was used to give an engine characteristic chamber length L* of 94 centimeters (37 in.). The heat-sink engine components are shown in figure 3.

Second, a water-cooled thrust chamber, shown in figure 8, was used for steady-state, long-duration firings to check injector durability and to obtain additional performance data. The water-cooled thrust chamber components are shown in figure 9. The 15-centimeter (6-in.) long water-cooled chamber section was also used upstream of the ablative and throat insert sections (discussed next) to bring the combined chamber length to 38 centimeters (15 in.). In addition, the water-cooled nozzle was used with cylindrical ablative chamber sections to measure injector-chamber compatibility during 300-second firings.

Third, a silica phenolic ablative thrust chamber was designed (fig. 10) to measure the influence of injector modification on ablative erosion characteristics. The material was manufactured to Fiberite MX 2646 specification, which includes chopped-square cloth reinforcement. In some tests, an ablative chamber section was used with the water-cooled nozzle to evaluate the effect of injector modifications on the tendency of

the injector pattern to erode the chamber wall.

Fourth, a thrust chamber with a throat insert and chamber liner was designed as illustrated in figure 11. The overall design was intended to prevent thrust chamber erosion for long-duration firings up to 1000 seconds of total firing time.

PROCEDURE

Engine Operation and Control

Before each firing, the propellant tanks were pressurized with nitrogen gas. Fire valve openings were automatically sequenced to provide an oxidant lead of approximately 0. 1 second. Individual automatic closed-loop controllers were used to maintain a constant chamber pressure and oxidant-to-fuel ratio. The run duration was controlled by an automatic timer. An automatic cutoff was used to terminate any firings when the throat area increase exceeded 25 percent. Emergency shutdowns were made manually if gas leakage or excessive erosion rates were noted.

Throat Measurements

New ablative and throat insert diameters were measured with a micrometer. After erosion or surface roughening, photographs were taken of the throat plane. The enlarged photographs were planimetered to obtain throat area after firing, and the areas were converted to an effective radius.

The effective throat radius change was also calculated during each firing from instantaneous values of chamber pressure and weight flow.

Calculations

The following calculations were made:

(1) Characteristic exhaust velocity efficiency ηC^* - An injector calibration firing was made for each injector with heat-sink hardware. The ηC^* values determined were then used to calculate ablative throat radius at any time as in calculation 3. No corrections were made to the C^* values to account for heat losses. (All symbols are defined in the appendix.)

$$\eta C^*_{P_c} = \frac{C^*_{exp}}{C^*_{theo}} \tag{1}$$

where C^*_{theo} is the theoretical one-dimensional shifting equilibrium characteristic velocity and

$$C^*_{exp} = \frac{\varphi P_{inj} C_d A_t g}{W_p}$$

(2) Momentum pressure loss correction, $(P_t/P_{inj}) = \varphi$

$$\varphi = \left(\frac{p_n}{P_n} + \frac{I_n g - v_{inj}}{C^*_{theo} \epsilon_{con}} \right)^{-1} \tag{2}$$

where v_{inj} is assumed to equal zero. Values of p_n/P_n, I_n, C^*_{theo} were obtained from theoretical data printouts performed by the methods of reference 9. Injection Mach numbers for the liquid propellants were sufficiently low to justify assumption of zero injection velocity. A value of 0.98 was calculated for φ.

(3) Effective throat radius change

(a) Throat radius at any time

$$R_{eff,\theta} = \sqrt{\frac{W_p \eta C^* C^*_{theo}}{\pi g \varphi P_{inj} C_d}} \tag{3a}$$

(b) Effective throat radius change at any time

$$\Delta R_{eff} = R_i - R_\theta \tag{3b}$$

(4) Characteristic chamber length

$$L^* = \frac{V_c}{A_t} \tag{4}$$

(5) Theoretical vacuum thrust coefficient efficiency

$$\eta C_{F,\,vac} = \frac{\lambda C_m C_{F,\,design} + \left(\frac{A_{ex}}{A_t}\right)\left(\frac{P_{ex}}{P_t}\right)}{C_{F,\,design} + \left(\frac{A_{ex}}{A_t}\right)\left(\frac{P_{ex}}{P_t}\right)} \tag{5}$$

(6) Vacuum specific impulse efficiency

$$\left.\begin{aligned} \eta I_{vac} &= \frac{I_{vac,\,exp}}{I_{vac,\,theo}} \\ I_{vac,\,exp} &= \frac{F_{vac}}{W_p} \\ F_{vac} &= F_{exp} + P_0 A_e \end{aligned}\right\} \tag{6}$$

(7) Experimental vacuum thrust coefficient efficiency

$$\eta C_{F,\,vac} = \frac{\eta I_{vac}}{\eta C^*_{P_c}} \tag{7}$$

(8) Characteristic velocity of an O/F-zoned injector

$$\left.\begin{aligned} C^*_{overall} &= \frac{W_{p,\,zone} C^*_{zone} + W_{p,\,core} C^*_{core}}{W_{p,\,zone} + W_{p,\,core}} = C^*_{exp} \\ C^*_{zone} &= \frac{C^*_{overall} W_{total} - C^*_{core} W_{p,\,core}}{W_{p,\,zone}} \end{aligned}\right\} \tag{8}$$

(9) Combustion temperature

$$T_{com} = T_{theo}\left(\frac{C^*_{exp}}{C^*_{theo}}\right)^2 \tag{9}$$

(10) Zone combustion gas temperature

$$T_{com,\,zone} = (\text{Theoretical } T_{com,\,zone,\,O/F})\left(\frac{C^*_{zone}}{\text{Theoretical } C^*_{zone,\,O/F}}\right)^2 \tag{10}$$

(11) Calculated vacuum specific impulse

$$I_{vac,\,calc} = (I_{vac,\,odk})(\eta C^*_{exp})(\eta C_{F,\,vac}) \tag{11}$$

(12) Discharge coefficient of oxidant injector (same method for fuel)

$$C_{d,\,ox} = \frac{W_{ox}}{A_{ox}\sqrt{\rho_{ox}\,\Delta P_{ox} 2g}} \tag{12}$$

(13) Mass flow rate of injector-zone oxidant (same method for fuel)

$$\left.\begin{aligned} W_{ox,\,zone} &= W_{ox,\,total} - W_{ox,\,core} \\ W_{ox,\,zone} &= W_{ox,\,total} - C_{d,\,ox,\,core} A_{ox,\,core}\sqrt{\rho_{ox}\,\Delta P_{ox} 2g} \end{aligned}\right\} \tag{13}$$

All theoretical values for these calculations were determined for these propellants by using the method of reference 11.

RESULTS AND DISCUSSION

The injector development program discussed herein was conducted to investigate means of obtaining a combustion gas environment compatible with advanced throat insert materials while maintaining high overall engine performance representative of state-of-the-art engines using earth-storable propellants. Ablative erosion rate and circumfer-

ential uniformity were used as parameters to evaluate the various injector modifications. The injector modifications that evolved are discussed in the order in which they were evaluated. The order of presentation of results is as follows: C^* performance, combustion temperature, vacuum specific impulse, and ablative erosion. Impulse performance data are presented first at low expansion area ratio; then to put the data into the perspective of a space engine, performance is corrected analytically to high area ratio. Finally, recommendations for improving performance with the same wall combustion environment as well as general methods for obtaining peak performance are included.

At the beginning of the program, two injectors (designated 1 and 2) were designed and tested (see table I). In figure 12 are the experimental C^* values for both injectors. The precision of the C^* values for this program was estimated at ±6.7 m/sec (±22 ft/sec), or ±0.4 percent ηC^* for one standard deviation. Injector 2 is seen to be about $1\frac{1}{2}$ percent more efficient than injector 1. The improved performance for injector 2 was attributed to better vaporization from the smaller holes and better mixing of the propellants by the mutually perpendicular triplets. Comparable results were noted for the larger injectors of reference 7. The calculated combustion temperatures based on measured performance values (see eq. (7)) for the two injectors are shown in figure 13, with injector 2 about 111 K (200° R) higher than injector 1. Extrapolated values, for later discussion, are shown by dashed portions on both curves.

The specific impulse values measured for both injectors at the low nozzle expansion area ratio used for testing ($\epsilon = 1.8$) are shown in figure 14. Losses from the theoretical one-dimensional equilibrium value were calculated by the simplified method given in reference 10. An approximation to the Interagency Chemical Rocket Propulsion Group (ICRPG) method also shown in figure 14 was that of equation (11):

$$I_{vac,\,calc} = (I_{vac,\,odk})(\eta C^*_{exp})(\eta C_{F,\,vac})$$

where C^* was derived from test measurement of chamber pressure. The thrust coefficient efficiency of 97.2 percent was obtained by theoretical calculation using equation (5). Careful thrust measurement over an extended series of test firings confirmed the thrust coefficient efficiency at 97.2±0.7 percent for one standard deviation.

Performance curves based upon low-area-ratio data were calculated for an engine with a conical nozzle ($\alpha = 15°$) at an expansion area ratio of 60, assuming that the thrust coefficient efficiency remained constant at 97.2 percent. The results are shown in figure 15.

The peak value of specific impulse for both injectors appears at an O/F of 1.55 for the low area ratio and at an O/F of 1.8 for the high area ratio. The difference was due to a shift in the one-dimensional kinetic peak theoretical performance, which occurs at an O/F of 1.8 for the high-area-ratio nozzle and at an O/F of 1.55 for the low-area-ratio

nozzle. Therefore, a realistic design must include kinetic losses and be based upon high-area-ratio impulse values. Accordingly, all further considerations of performance are reflected against a map of one-dimensional kinetic theoretical curves for high-area-ratio nozzles. Specific values are calculated by the expression $I_{vac} = (I_{vac,\,odk})(\eta C_F)\left(\eta C^*_{P_c}\right)$ where a constant value of $\eta C_F = 0.972$ was used.

The results of testing both injectors with ablative nozzles are given by the throat erosion curves of figure 16. The steady-state erosion rates along with the times to start erosion are tabulated in table II. The steady-state erosion rate is calculated from the slope of the erosion curve. The calculation of equation (3b) assumes a circular flow area; and thus, the results were called effective throat radius change. An estimate of the degree of gouging present may be made by referring to the circular reference disk for each injector. The time to start erosion was defined as the time when erosion exceeds material expansion and first becomes positive.

The significant influence of injector design is illustrated by the $1\frac{1}{2}$ percent efficiency advantage of injector 2 with essentially the same ablative throat erosion rate as injector 1. Overall heat transfer at the throat must have been similar, although the calculated combustion temperature for injector 1 was 110 K (200° R) below that of injector 2. Coarser elements and orientation providing less mixing for injector 1 were thought to account for the heat-transfer similarity at different efficiency levels.

The ablative throat erosion rate was unsatisfactorily high with both of these injectors (0.013 cm/sec; 0.005 in./sec); however, the low-cost ablative used was not the most erosion resistant (ref. 1). Further, the temperature of 2977 K (5358° R) for injector 2 was high enough to melt and destroy catastrophically in 225 seconds one of the more advanced inserts (ZrO_2) intended for 700-second firing (ref. 3). Although not fired with a throat insert, injector 1 would probably have produced similar results based upon its ablative throat erosion characteristics. In order to proceed with insert testing, a lower gas temperature adjacent to the chamber wall was needed. Based on previous experience (ref. 7), it was determined that combustion temperatures of 2660 to 2720 K (4800° to 4900° R) would be low enough to prevent melting of inserts but still high enough to give the desired impulse performance.

An effective format for studying the tradeoffs of performance and combustion temperature is shown in figure 17. Plotted here is the theoretical one-dimensional kinetic vacuum specific impulse (100 percent ηI_{sp}) against theoretical combustion temperature as each is affected by varying the propellant mixture ratio (O/F). Shown also is the desired performance and temperature goal as a region bounding I_{sp} values greater than 3016 N-sec/kg (307.5 lbf-sec/lbm) and temperature less than 2720 K (4900° R). It is obvious that the desired performance could be attained with 100 percent ηI_{sp} over a limited range of O/F values below 1.8. Methods considered for reaching the desired performance are the following: (1) decrease the overall O/F, (2) decrease injector effi-

TABLE II. - INJECTOR PERFORMANCE AT OVERALL OXIDANT-TO-FUEL RATIO OF 2.0

(a) SI units

Injector			Location of propellant mass	Percent of propellant flow	Mixture ratio, O/F	Characteristic exhaust velocity, C^*			Vacuum specific impulse, I_{vac}			Combustion temperature, K	Erosion	
Designation	Type	Pattern				Theoretical, m/sec	Experimental, m/sec	ηC^*, percent of theoretical	Theoretical (one-dimensional kinetic), N-sec/kg	Calculated, N-sec/kg	ηI, percent of theoretical		Steady-state rate, cm/sec	Time to start, sec
1	Triplet (fuel on oxidant)	Circular	Core	100	2.00	1712	1642	95.90	3267	3045	93.21	2874	0.0127	12
			Zone	0	----	----	----	-----	----	----	-----	----		
			Overall	100	2.00	1712	1642	95.90	3267	3045	93.21	----		
2	Triplet (fuel on oxidant)	Mutually perpendicular grid	Core	100	2.00	1712	1671	97.60	3267	3099	94.87	2975	0.0132	17
			Zone	0	----	----	----	-----	---	---	-----	----		
			Overall	100	2.00	1712	1671	97.60	3267	3099	94.87	----		
2A	Triplet (low O/F zone on outside)	Mutually perpendicular grid with zone	Core	69.83	2.55	1636	1599	97.60	3137	2976	94.87	2993	0.0048	64
			Zone	30.17	1.21	1722	1686	97.96	3143	2993	95.22	2663		
			Overall	100	2.00	1712	1626	95.00	3267	3016	92.34	----		
2B	Triplet (all outer elements radial)	Mutually perpendicular grid with radial zone	Core	73.45	2.30	1671	1631	97.60	3204	3039	94.87	2964	0.0076	39
			Zone	26.55	1.40	1740	1677	96.37	3218	3014	93.67	2737		
			Overall	100	2.00	1712	1643	95.99	3267	3048	93.31	----		
2C	Triplet and quadlet (all outer elements arranged three fuel holes on one oxidant hole)	Mutually perpendicular grid with radial zone	Core	69.84	2.45	1650	1610	97.60	3167	3004	94.87	2949	0.0053	42
			Zone	30.16	1.31	1733	1680	96.37	3189	3006	94.25	2700		
			Overall	100	2.00	1712	1631	95.30	3267	3026	92.63	----		

TABLE II. - Concluded. INJECTOR PERFORMANCE AT OVERALL OXIDANT-TO-FUEL RATIO OF 2.0

(b) U. S. customary units

Injector			Location of propellant mass	Percent of propellant flow	Mixture ratio, O/F	Characteristic exhaust velocity, C^*			Vacuum specific impulse, I_{vac}			Combustion temperature, ^oR	Erosion	
Designation	Type	Pattern				Theoretical, ft/sec	Experimental, ft/sec	ηC^*, percent of theoretical	Theoretical (one-dimensional kinetic), lbf-sec/lbm	Calculated, lbf-sec/lbm	ηI, percent of theoretical		Steady-state rate, in./sec	Time to start, sec
1	Triplet (fuel on oxidant)	Circular	Core	100	2.00	5616	5386	95.90	333.1	310.5	93.21	5173	0.0050	12
			Zone	0	----	----	----	----	-----	-----	-----	----		
			Overall	100	2.00	5616	5386	95.90	333.1	310.5	93.21	----		
2	Triplet (fuel on oxidant)	Mutually perpendicular grid	Core	100	2.00	5616	5481	97.60	333.1	316.0	94.87	5356	0.0052	17
			Zone	0	----	----	----	-----	-----	-----	-----	----		
			Overall	100	2.00	5616	5481	97.60	333.1	316.0	94.87	----		
2A	Triplet (low O/F zone on outside)	Mutually perpendicular grid with zone	Core	69.83	2.55	5366	5247	97.60	319.9	303.5	94.87	5387	0.0019	64
			Zone	30.17	1.21	5648	5533	97.96	320.5	305.2	95.22	4793		
			Overall	100	2.00	5616	5335	95.00	333.1	307.6	92.34	----		
2B	Triplet (all outer elements radial)	Mutually perpendicular grid with radial zone	Core	73.45	2.30	5482	5351	97.60	326.7	309.9	94.87	5335	0.0030	39
			Zone	26.55	1.40	5710	5503	96.37	328.1	307.3	93.67	4927		
			Overall	100	2.00	5616	5391	95.99	333.1	310.8	93.31	----		
2C	Triplet and quadlet (all outer elements have three fuel holes on one oxidant hole)	Mutually perpendicular grid with radial zone	Core	69.84	2.45	5413	5283	97.60	322.9	306.3	94.87	5308	0.0021	42
			Zone	30.16	1.31	5685	5513	96.97	325.2	306.5	94.25	4861		
			Overall	100	2.00	5616	5352	95.30	333.1	308.6	92.63	----		

ciency, (3) apply fuel film cooling to the periphery of the combustion gases, and (4) apply a low O/F zone to the periphery of the combustion gases. Each of these methods is discussed in detail in the following paragraphs.

(1) Decrease the overall O/F - The influence of O/F variation on combustion temperature and performance level is further illustrated in figure 18. The upper curve was calculated for a thrust coefficient efficiency of 97.2 percent and a C^* efficiency of 100 percent as a reference. It is seen that increasing O/F does not reduce the temperature sufficiently at the desired performance level. Decreasing O/F does allow operation at both the desired performance and temperature levels if high C^* efficiency can be maintained. Extrapolation of the performance data for injectors 1 and 2 in figures 13 and 15 shows the O/F operating points necessary to achieve the desired temperature. These extrapolated curves are plotted in figure 18 for both injectors. Both injectors fall below the desired performance level, even though ηC^* values were 96 to 97 percent. Injector 2, however, would nearly meet both requirements at an O/F of about 1.3. As a practical alternative for existing spacecraft, an O/F of 1.3 is probably too low because of bulk density considerations. Based upon this discussion, decreasing the overall O/F was discarded from further consideration.

(2) Decrease injector C^* efficiency - Figure 19 illustrates the effect of a decrease in injector efficiency at an O/F of 2. The top point represents theoretical one-dimensional kinetic performance with an expansion area ratio of 60. Thrust coefficient efficiencies (97.2 percent used herein) do not affect combustion gas temperature but lower the available performance to 3174 N-sec/kg (323.7 lbf-sec/lbm) for 100 percent C^* performance. Temperatures at lower C^* values (calculated by eq. (9)) are marked on the curve with the actual performance of injectors 1 and 2 shown. It can be seen that the desired goal cannot be met by this means.

(3) Apply film cooling to the periphery of the combustion gases - All the methods considered up to now have attempted to meet the performance objective by bringing all the combustion gases to the desired temperature and specific impulse values. An alternative would be to divide the flow in the thruster into two regions: one adjacent to the wall with the temperature depressed, and the other in the center of the thruster with specific impulse maximized. One method of doing this is with film cooling. In this case, the region (or zone) adjacent to the wall is composed of only fuel, quite cool but of limited thickness and axial extent and quite low in specific impulse. In order to optimize this method, the flow in the fuel zone must be precisely tailored to produce the desired cooling at the throat plane with as low a fuel flow as possible. Fuel film cooling shows some promise, but was considered to be a specialized form of the method discussed next.

(4) Applying a low O/F zone to the periphery of the combustion gases - A more general form of combustion gas flow stratification is O/F zoning. Selection of this method was based upon two aspects. The first is that a very cool (such as film cooled) zone is

not entirely necessary since a temperature of 2660 to 2720 K (4800° to 4900° R) is tolerable with the chamber materials in question. A zone of 2660 to 2720 K (4800° to 4900° R) would also have less performance loss than a cooler zone. Application of an O/F zone between 1.2 and 1.4 to the periphery of the injector would provide the desired temperature if sufficient mass flow were used to completely blanket the higher temperature core. The second aspect involves minimizing the mixing between the two zones. The velocity difference between core flow and peripheral-zone flow is less in the case of O/F zoning than it is with film cooling. Hence, one would expect less mixing and better maintenance of the zone cooling influence throughout the length of the chamber.

The O/F zoning technique seemed the most promising for controlling boundary temperatures while maintaining high delivered specific impulse. It was, therefore, decided to modify injector 2 by O/F zoning.

The first modification was accomplished by increasing fuel flow area in the outer row of 36 elements of injector 2, as shown in figure 4(a). For these tests, overall operating O/F was 2.0. Therefore, the core O/F was raised to compensate for the low O/F zone. Reasons for operation at an overall O/F of 2.0 included illustration of significant effects under overall operation at the temperature peak, compatibility with contemporary spacecraft tankage, and comparison with previous insert development done at an O/F of 2.0 (ref. 2).

The various modifications to injector 2 and their results are tabulated in table II. Mass flow rates in the core and zone were calculated for each modification by using equations (10) and (11). Basically, the method calculates discharge coefficients C_d for the unmodified injector oxidant and fuel as in equation (10). The core flow rate for the modified injector is calculated as in equation (11) assuming no change in core discharge coefficient. Measured pressure drops and core flow areas are used for core flow calculations. Values are subtracted to give zone flows, and the respective O/F values are derived. Precision of the calculations has been estimated at ±1.2 percent for one standard deviation on the weight flow split W_{zone}/W_{total} and ±1.7 percent for one standard deviation on O/F ratio. Some of the spread in the values may be due to the assumption that the measured pressure drop across the injector face during propellant flow applies equally to both core and zone.

The initial modification (injector 2A) was to enlarge the fuel holes in the outer 36 elements from 0.046-centimeter (0.018-in.) diameter to 0.061-centimeter (0.024-in.) diameter. The flow calculations then indicated that for an overall O/F of 2.0, 30 percent of the mass flow would be in the outer zone at an O/F of 1.22 and 70 percent of the mass flow would be in the core with an O/F of 2.55.

When injector 2A was tested at an overall O/F of 2.0, an overall C^* of 1626 m/sec (5335 ft/sec) was determined from measured values. In order to calculate the zone C^*, it was necessary to know the core C^*. It was assumed that the core C^* remained at

97.6 percent efficiency, as it was with the unmodified injector. Thus, for the O/F of 2.55 calculated for the core, the assumed core C^* was 1599 m/sec (5247 ft/sec). Equation (8), which was used to calculate zone C^*, assumes zero mixing between zone and core. Equation (8) is of the form

$$C^*_{overall} = C^*_{exp} = (\text{Mass fraction of zone})(C^*_{zone}) + (\text{Mass fraction of core})(C^*_{core})$$

In SI units,

$$1626 = 0.3017(C^*_{zone}) + 0.6983(1599)$$

$$1626 = 0.3017\ C^*_{zone} + 1117$$

$$C^*_{zone} = 1687 \text{ m/sec}$$

In U. S. customary units,

$$5335 = 0.3017(C^*_{zone}) + 0.6983(5247)$$

$$5335 = 0.3017\ C^*_{zone} + 3664$$

$$C^*_{zone} = 5535 \text{ ft/sec}$$

This calculation illustrates that 30 percent of the overall C^* is the zone contribution and 70 percent of the overall C^* is in the core contribution.

The measured, assumed, and calculated C^* values are given in figure 20. The relation between these values for zero mixing is illustrated by the straight line connecting the points. The data generally support the zero-mixing criterion. If 100-percent mixing between zone and core were to occur in the rocket combustion chamber after injection, the upper dashed line in figure 20 would give the locus of points for overall C^* at any mass split from 100-percent core to 100-percent zone. For our particular case where 70 percent of the mass flow was at the core O/F and 30 percent of the mass flow was at the zone O/F, perfect mixing would produce a C^* of about 1670 m/sec (5480 ft/sec) at an overall O/F of 2.0. Of course, 100 percent mixing by the time the gases reach the throat would also eliminate the temperature protection desired from the O/F zoning. The influence of choosing O/F values on both sides of the performance peak is also illustrated in figure 20. Note that core and zone are both operating at high efficiency (above 97 percent) but the overall efficiency of the combination is only 95 percent. Changing the mass split between core and zone would only move the overall C^*

along the dashed line so that, if no mixing occurs, the overall efficiency is always below the zone-core efficiencies. Again, this is due to zone-core O/F placement on both sides of the C* peak O/F.

The calculations for specific impulse values involved multiplying the theoretical one-dimensional kinetic impulse by characteristic velocity efficiency and the vacuum thrust coefficient efficiency (97.2 percent). The calculation was done independently for zone, core, and overall O/F points and resulted in the slightly curved line for injector 2A (fig. 21). The influence of placing the zone and core O/F on both sides of the performance peak is seen to reduce overall efficiency below both the zone and core efficiency.

The temperatures for injector 2A (fig. 22) are calculated by applying the zone and core $(\eta C^*)^2$ values to the theoretical combustion temperature. The core was operating at 2937 K (5287° R) and the zone was operating at 2664 K (4795° R). This zone provided the low end of the 2660 to 2720 K (4800° to 4900° R) temperature range desired. The steady-state ablative throat erosion rate was 0.005 cm/sec (0.002 in./sec), which also was a significant improvement over 0.013 cm/sec (0.005 in./sec) with unmodified injector 2. The erosion pattern, however, was somewhat irregular (see fig. 23). Therefore, it was decided to try to eliminate the circumferential irregularity of the ablative erosion and, at the same time, attempt to improve delivered vacuum specific impulse.

The irregular ablative erosion experienced with injector 2A appeared to be caused by zone injector elements that were parallel to the wall in some areas and perpendicular to the wall in other areas. To overcome this, the injector elements in the outer zone of injector 2B (fig. 5(b)) were oriented in a radial pattern which generated spray fans in a circumferential direction (parallel to the wall). In order to improve the delivered specific impulse, the O/F ratio in the zone was increased to 1.40 (from 1.22 for injector 2A) by decreasing the hole size of the fuel holes in the outer zone. Where possible (all but six elements), the fuel holes on the outer elements were reduced from the 0.061-centimeter (0.024-in.) diameter of injector 2A by one drill size to 0.057-centimeter (0.0225-in.) diameter. This gave a calculated zone O/F of 1.40 and an O/F of 2.30 in the core, with the overall O/F of 2.0. The mass flow split was also changed slightly to 73 percent in the core and 27 percent in the zone.

Injector 2B was tested at an overall O/F of 2.0, and a C* of 1643 m/sec (5391 ft/sec) was calculated from test measurements. The C* operating points are plotted in figure 24. A core C* of 1631 m/sec (5351 ft/sec), based upon an extrapolation of the calibration firings of the original injector to an O/F of 2.3, was used to calculate a C* of 1677 m/sec (5503 ft/sec) for the outer zone.

The data for injector 2B's specific impulse are shown in figure 25. The overall value was 3048 N-sec/kg (310.8 lbf-sec/lbm). This was an increase of 31.4 N-sec/kg (3.2 lbf-sec/lbm) from injector 2A, due mainly to operating both core and zone closer to the performance peak.

The combustion temperatures calculated for the core and the zone are plotted in figure 26. With the core temperature at 2964 K (5335° R), the zone temperature was 2737 K (4927° R). Thus, the increase of 31.4 N-sec/kg (3.2 lbf-sec/lbm) in specific impulse was achieved with a 74 K (134° R) increase in zone temperature compared to injector 2A. The temperature was still 238 K (429° R) below that of the original injector.

The influence of these modifications on ablative erosion is illustrated in figure 27. Although the erosion pattern was somewhat more uniform, the steady-state erosion rate was 0.0076 cm/sec (0.003 in./sec), still less that injector 2 but higher than injector 2A. The erosion rate and zone temperature seemed too high for the projected throat insert testing.

Consequently, it was decided to make a further modification to try to decrease the outer zone temperature while maintaining the highest possible specific impulse. The basic objective was to decrease zone O/F somewhat and also to blanket the oxidant more completely with fuel. The outer elements were revised by substituting two fuel holes for each single outer fuel hole to the particular elements shown in figures 6(c) and (d). A jet spreading angle of 12° was used to place the streams for complete coverage of the oxidant by the fuel. The impact area of the additional outer two fuel streams was made significantly larger than the impact area of the inner fuel stream in an attempt to produce a bent spray fan pattern more nearly parallel to the curved wall. The calculated values for injector 2C are listed in table II. The mass split was 70 percent in the core at an O/F of 2.45 and 30 percent in the outer zone at an O/F of 1.31. This O/F should place the zone temperature lower than the 2737 K (4927° R) of injector 2B but above the 2663 K (4793° R) of injector 2A.

When injector 2C was tested at an overall O/F of 2.0, a C^* of 1631 m/sec (5352 ft/sec) was calculated from test measurements. The zone operating points are plotted in figure 28. Assuming the original core ηC^* of 97.6, a value of 1680 m/sec (5513 ft/sec) was calculated for the zone C^*. Again, both zone and core C^* efficiencies were higher than the overall efficiency because their operating O/F's were on both sides of the performance peak O/F.

The specific impulse for injector 2C is shown in figure 29. A value of 308.6 seconds was calculated from measurements at an overall O/F of 2.0. This was between the values for injector 2A (307.6 sec) and injector 2B (310.8 sec), as expected. The same efficiency loss caused by zone and core operation on opposite sides of the performance peak is illustrated.

Another way of calculating the performance loss due to O/F zoning is given in reference 11. When the ICRPG method was applied to the data of injector 2, a mixture ratio distribution loss of 66 N-sec/kg (6.8 lbf-sec/lbm) was calculated for injector 2C at an O/F of 2.0. This compares to the loss of 72 N-sec/kg (7.4 lbf-sec/lbm) calculated by

the constant thrust coefficient efficiency method used herein. Agreement was well within the precision expected from both methods.

The temperature points for injector 2C are shown in figure 30. The core is at 2949 K (5308° R). The zone is at 2700 K (4861° F) - between the 2663 K (4793° R) of injector 2A and the 2737 K (4927° R) of injector 2B, with a reduction of 275 K (495° R) from the unmodified injector 2.

Ablative testing produced throat erosion, as shown in figure 31, with a steady-state rate of 0.0053 cm/sec (0.0021 in./sec). The ablation rate seemed to be a reasonable compromise although the pattern was still nonuniform. Since the impulse loss of 72.6 N-sec/kg (7.4 lbf-sec/lbm) for injector 2C relative to injector 2 was reasonable for the 275 K (495° R) temperature decrease, a tentative decision was made to proceed with throat insert testing.

Prior to insert testing, however, a test firing was made with injector 2C and an instrumented heat-sink nozzle to provide an experimental check on the temperatures calculated from the C* and O/F values. Open bead tungsten/tungsten-rhenium thermocouples of 0.097-centimeter (0.038-in.) bead diameter were inserted at different depths into the combustion gas at the rocket throat. It was possible to measure steady-state temperature outputs during 5-second test firings prior to thermocouple burnout. The values in figure 32 illustrate the measured temperatures through the peripheral zone of the combustion stream at the nozzle throat. Gas temperature at each depth was measured by three thermocouples spaced at 120° intervals. For the engine size tested herein, a zone that would carry 30 percent of the mass flow through the throat would be 0.617 centimeter (0.243 in.) thick at the throat. The comparison of the temperatures measured at 0.457 and 0.610 centimeter (0.180 and 0.240 in.) from the wall agreed very well with the calculated values, which verified the presence of temperature zoning. Near the wall, the measured temperature was significantly below the calculated zone temperature, probably due to heat transfer to the heat-sink nozzle wall from both the thermocouple and the gas it was trying to measure. Another possible cause of the depressed temperature at the wall of the nozzle could be reduced chemical activity due to "kinetic quenching." Although the measurements were done in a heat-sink chamber, a temperature depression is also known to exist in ablative engines due to ablation and the flow of pyrolysis gases from the wall. In any event, these measurements provided confidence in the design process so that throat insert testing could commence.

The results of throat insert testing were reported in reference 3, and a significant decrease in temperature was confirmed. Figure 33(a) (fig. 27 of ref. 3) illustrates the beneficial influence of the injector modification on the life of identical zirconia throat inserts. It should be noted that throat inserts of significantly better materials are also reported in reference 3. Testing of an ablative chamber section for long duration also confirmed that a less severe local combustion temperature was present in the chamber

with injector 2C. The contrasting appearance of the ablative chamber sections is shown in figures 33(b) and (c).

A correlation of the ablative erosion with temperature for injector 2 and its modifications is given in figure 34. The erosion data from table II summarized here show a definite dependency of erosion on peripheral-zone combustion temperature. The curve of steady-state erosion rate extrapolates to zero erosion at a temperature of 2481 K (4465° R). The curve of time to start erosion is approaching a vertical asymptote at the same temperature. This agrees with previous experience for zero erosion with ηC^* below 90 percent at an O/F = 2.0 (T_c = 2533 K or 4560° R).

The influence on performance of various methods for decreasing peripheral-zone temperature is illustrated in figure 35. The O/F zoning method is seen to give significant performance gain over the efficiency-decrease method of temperature suppression.

The method of overall O/F decrease does provide performance only 2.5 seconds below that of injector 2C. Coupled with increased propellant storage (tankage) weight required by low O/F operation, the vehicle performance loss would be significant, however.

METHOD OF APPLICATION

Before a detailed rocket engine design can be attempted, several important goals must be specified. The most significant is the vacuum specific impulse required from the particular propellant combination used.

Chamber pressure and expansion area ratio values must be set to derive theoretical vacuum specific impulse. The theoretical impulse values must be modified for kinetic losses, geometrical losses, and viscous and heat-transfer losses before proceeding with injector design. A method for measuring or calculating vacuum thrust coefficient efficiency $\eta C_{F, vac}$ is required to derive nozzle losses. A method for calculating or estimating characteristic exhaust velocity efficiency ηC^* is required to determine energy release losses. When these losses were accounted for, the vacuum specific impulse for injector 2 peaked at an O/F of 1.8 and a value of 3109 N-sec/kg (317 lbf-sec/lbm) (fig. 15). Using injector 2 at any O/F other than 1.8 involves a loss of specific impulse, which must be recognized. Even use of the unmodified injector at an O/F of 2.0, as shown in figure 13, involves a loss of 1 second of impulse. Further, O/F zoning with an overall O/F of 2.0 produces impulse losses, as shown in figure 35. To maximize specific impulse, injector 2 should be operated at an O/F of 1.8. Since this would produce too high a combustion temperature (2944 K or 5300° R), some form of peripheral cooling is necessary. To keep delivered impulse as high as possible, the core O/F should be 1.8. Three hypothetical cases (A, B, and C) were calculated based upon a core O/F

of 1.8 (see table III). Each case was selected at a zone O/F of interest to show the influence of temperature variation upon performance. Figure 36 illustrates the range of values calculated. All calculations were done for a 70-percent - 30-percent mass split, which provides sufficient peripheral-zone temperature control for ablative-insert protection at the scale tested. Overall impulse values were based upon the core remaining at its original C^* efficiency of 97.6 percent for an O/F of 1.8. In order to confirm the general trend of performance for a core O/F of 1.8, a measured point (circular symbol) was included in figure 36 for injector 2C operating with its core at 1.8 O/F and an overall O/F of 1.47. The zone O/F was 0.96 at a calculated zone temperature of 2000 K (3600° R), which was too low for this throat insert investigation but may be of interest for rocket vehicle systems requiring lower temperatures. Figure 37 illustrates the trend of zone element C^* efficiency with decreasing O/F. Since these elements were designed to operate at an O/F of 1.31, the efficiency decrease was not unexpected. A design for lower O/F - lower temperature operation could provide higher efficiency

TABLE III. - INJECTOR PERFORMANCE AT CORE OXIDANT-TO-FUEL RATIO OF 1.8

(a) SI units

Injector	Location of propellant mass	Percent of propellant flow	Mixture ratio, O/F	Characteristic exhaust velocity, C^*			Vacuum specific impulse, I_{vac}			Combustion temperature, K
				Theoretical, m/sec	Calculated, m/sec	ηC^* percent of theoretical	Theoretical (one-dimensional kinetic), N-sec/kg	Calculated, N-sec/kg	ηI, percent of theoretical	
Hypothetical injectors										
A	Core	70	1.800	1702	1691	97.60	3280	3112	94.87	2958
	Zone	30	1.600	1742	1705	97.60	3262	3094	94.87	2916
	Overall	100	1.737	1736	1694	97.56	3279	3110	94.83	----
B	Core	70	1.800	1702	1691	97.60	3280	3112	94.87	2958
	Zone	30	1.310	1734	1679	96.97	3189	3006	94.25	2700
	Overall	100	1.632	1740	1687	96.95	3268	3079	94.24	----
C	Core	70	1.800	1702	1691	97.60	3280	3112	94.87	2958
	Zone	30	1.120	1706	1611	94.52	3095	2843	91.87	2387
	Overall	100	1.554	1741	1666	95.70	3254	3026	93.02	----
Actual injector										
2C	Core	68.87	1.800	1702	1691	97.60	3280	3112	94.87	2958
	Zone	31.13	.961	1666	1521	91.33	2993	2657	88.77	2041
	Overall	100.00	1.471	1741	1637	94.00	3236	2957	91.37	----

TABLE III. - Concluded. INJECTOR PERFORMANCE AT CONE OXIDANT-TO-FUEL RATIO OF 1.8

(b) U. S. customary units

Injector	Location of propellant mass	Percent of propellant flow	Mixture ratio, O/F	Characteristic exhaust velocity, C^*			Vacuum specific impulse, I_{vac}			Combustion temperature, ^oR
				Theoretical, ft/sec	Calculated, ft/sec	ηC^*, percent of theoretical	Theoretical (one-dimensional kinetic), lbf-sec/lbm	Calculated, lbf-sec/lbm	ηI, percent of theoretical	
Hypothetical injectors										
A	Core	70	1.800	5686	5550	97.60	334.5	317.3	94.87	5325
	Zone	30	1.600	5718	5581	97.60	332.6	315.5	94.87	5249
	Overall	100	1.737	5698	5559	97.56	334.4	317.1	94.83	----
B	Core	70	1.800	5686	5550	97.60	334.5	317.3	94.87	5325
	Zone	30	1.310	5685	5513	96.97	325.2	306.5	94.25	4861
	Overall	100	1.632	5713	5539	96.95	333.2	314.0	94.24	----
C	Core	70	1.800	5686	5550	97.60	334.5	317.3	94.87	5325
	Zone	30	1.120	5600	5293	94.52	315.6	289.9	91.87	4297
	Overall	100	1.554	5719	5473	95.70	331.8	308.6	93.02	----
Actual injector										
2C	Core	68.87	1.800	5686	5550	97.60	334.5	317.3	94.87	5325
	Zone	31.13	.961	5466	4992	91.33	305.2	270.9	88.77	3674
	Overall	100.00	1.471	5719	5376	94.00	330.0	301.5	91.37	----

operation of the zone elements and thus improve upon zone element efficiency at 1.12 and 0.96 O/F. The advantage of operating the core at peak performance O/F over operation at an overall O/F of 2.0 is illustrated in figure 38. The best operating point for injector 2 is an O/F of 1.8 at a specific impulse of 3112 N-sec/kg (317.3 lbf-sec/lbm). Modification to injector 2C for operation at an overall O/F of 2.0 reduces performance to 3025 N-sec/kg (308.5 lbf-sec/lbm) even though both zone and core are operating nearly as efficiently as before. This is because zone and core performance are on opposite sides of the performance peak with the overall performance on approximately a straight line between the two. A better method would be that of hypothetical injector B, where the core is at an O/F of 1.8 and the zone at 1.3, requiring an overall O/F of 1.65 for the 70-percent - 30-percent mass split assumed. A specific impulse gain of 53.9 N-sec/kg (5.5 lbf-sec/lbm) is seen over injector 2C.

One way to improve upon the overall delivered impulse of hypothetical injector B and still maintain the 2685 K (4834^o R) boundary gas temperature (O/F = 1.31) would be to increase the mass of propellant in the core and decrease the mass of propellant in

the zone. This moves the overall O/F toward 1.8 along the dashed line, thus increasing overall performance. Experiments to measure boundary-layer temperatures, as well as ablative nozzle firings, are necessary to determine the influence of mass variation.

A further point of interest in figure 38 is the operation of injector 2C at an overall O/F of 1.47 with the core at an O/F of 1.8 and the zone at an O/F of 0.96. The performance loss of 137 N-sec/kg (14 lbf-sec/lbm) I_{sp} was measured with a calculated peripheral-zone temperature of 2008 K (3614^{o} R) (fig. 36). Based upon figure 34, this zone temperature would be expected to provide zero ablative erosion for long-duration firings. If performance losses of 137 N-sec/kg (14 lbf-sec/lbm) are acceptable in return for elimination of ablative erosion or in lieu of complex throat insert systems, the tradeoff could be made as in figure 36. Further determination of the temperature-performance curve to lower temperatures would best be done experimentally. The influence of gross temperature differences, as well as gross O/F differences, might affect the mass of propellants required to effectively blanket the core with a low-temperature zone.

CONCLUDING REMARKS

In designing an injector to generate a zoned O/F distribution in the combustion chamber, several guidelines are obvious:

(1) Select the core O/F at the point of maximum vacuum specific impulse at high expansion area ratio if performance is the only consideration.

(2) Select the zone O/F to provide the desired wall environment, recognizing that the further it is away from the maximum performance O/F, the lower the combined performance will be.

(3) To maximize overall impulse with the core at maximum specific impulse O/F, make the core mass flow as large a percentage of the total as possible without diluting the zone O/F influence on the wall. In the present case, 70-percent mass flow in the core was effectively blanketed by 30-percent mass flow in the zone, but these values were not necessarily optimum and would likely vary for other engine sizes.

(4) Discourage mixing between zone and core. Distribute the mass flow of both zone and core uniformly across the injector face with a maximum number of elements of a minimum practical size. Avoid all recirculation flows or radial or circumferential momentums (after impingement).

SUMMARY OF RESULTS

The influence of combustion gas flow stratification on overall engine performance, as well as on ablative and throat insert performance, was measured. The test engine was a rocket engine with a 7.62-centimeter (3.0-in.) throat diameter using earth-storable propellants at a chamber pressure of 690 kN/m^2 (100 psia). The following results were obtained:

1. Combustion gas temperature measurements and ablative throat erosion rates indicated that the combustion products from a rocket thruster of 4450-N (1000-lbf) size can be divided and generally maintained in two discrete zones through the throat region.

2. With 70 percent of the mass flow in the core and 30 percent of the mass flow in the outer zone, a significant influence on the ablative erosion can be obtained by maintaining an overall oxidant-to-fuel mixture ratio (O/F) of 2.0 and setting the core O/F at 2.3 to 2.5 and the zone O/F at 1.4 to 1.2.

3. A direct correlation for the data reported herein exists between ablative erosion rate (as well as time for erosion to start) and combustion temperature in the outer zone as determined by zone O/F and characteristic exhaust velocity efficiency ηC^*. A zone temperature of 2700 K (4861° R) at an O/F of 1.31 produced improved ablation results with the core operating at 2949 K (5308° R) and an O/F of 2.45.

4. For the same peripheral combustion temperature, O/F zoning allows higher specific impulse than simply decreasing overall injector efficiency. For O/F zoning and an overall O/F of 2.0, overall vacuum specific impulse is a function of temperature in the peripheral zone. At a desired zone temperature of 2700 K (4861° R), a value of 3026 N-sec/kg (308.6 lbf-sec/lbm) (nozzle area expansion ratio $\epsilon = 60$) was achieved with an overall O/F of 2.0.

5. Based upon the work reported herein, an optimum system for O/F zoning would include operation of the core at the O/F for peak impulse and a minimum percent of mass flow in the zone. Ablative thrust chambers and peripheral-zone measurements on heat-sink engines are useful tools for evaluation of zoned injectors.

Lewis Research Center,
National Aeronautics and Space Administration,
Cleveland, Ohio, May 17, 1972,
113-31.

APPENDIX - SYMBOLS

A	area, cm^2; $in.^2$
C^*	characteristic exhaust velocity, m/sec; ft/sec
C_d	flow coefficient (0.991 - Kliegel-Levine curve of ref. 11)
C_F	thrust coefficient
C_m	momentum coefficient $\left(\text{equals } C_d^2\right)$
D	diameter, cm; in.
F	thrust, N; lbf
g	gravitational constant, 9.8 m/sec^2; 32.174 ft/sec^2
I	specific impulse, N-sec/kg; lbf-sec/lbm
L^*	characteristic chamber length, cm; in.
O/F	oxidant-to-fuel weight mixture ratio
P	total pressure, kN/m^2; psi (absolute)
ΔP	injector pressure drop, N/m^2; $lbf/in.^2$
p	static pressure, kN/m^2; psi (absolute)
R	throat radius, cm; in.
ΔR	throat radius change, cm; in.
T	temperature, K; ^oR
V	volume, cm^3; $in.^3$
v	velocity
W	mass flow rate, kg/sec; lbm/sec
α	nozzle divergence half-angle, deg
β	jet spreading angle, deg
ϵ	nozzle expansion area ratio
η	efficiency, percent
λ	nozzle divergence correction, $1/2(1 + \cos \alpha)$
π	3.1416
ρ	density, kg/m^3; lbm/ft^3
φ	momentum pressure loss correction

Subscripts:

c	chamber
calc	calculated
com	combustion
con	contraction
d	discharge
e	expansion
eff	effective
exp	experimental
ex	exit (nozzle)
f	fuel
i	initial
inj	injector
n	subsonic nozzle entrance
odk	one-dimensional kinetic
ox	oxidant
p	propellant
t	throat
theo	theoretical equilibrium
vac	vacuum
θ	time
0	ambient

REFERENCES

1. Pavli, A. J.: Experimental Evaluation of Several Advanced Ablative Materials as Nozzle Sections of a Storable-Propellant Rocket Engine. NASA TM X-1559, 1968.
2. Winter, Jerry M.; and Peterson, Donald A.: Development of Improved Throat Inserts for Ablative Rocket Engines. NASA TN D-4964, 1969.
3. Winter, Jerry M.; Peterson, Donald A.; Shinn, Arthur M., Jr.; and Pavli, Albert J.: Development and Testing of an Ablative Rocket Engine with Selected 7.62-Centimeter (3.0 In.) Diameter Throat Inserts. NASA TM X-2315, 1971.
4. Aukerman, Carl A.; and Trout, Arthur M.: Experimental Rocket Performance of Apollo Storable Propellants in Engines with Large Area Ratio Nozzles. NASA TN D-3566, 1966.
5. Johnson, R. J.: Investigation of Thrusters for Cryogenic Reaction Control Systems. Vol. 1. Rep. TRW-09849-6001-RO-00-VOL-1, TRW Systems Group (NASA CR-72784), Nov. 13, 1970.
6. Senneff, John M.: Designing for Zonal Combustion. Rep. S-155243.6, Bell Aerosystems Co.
7. Winter, Jerry M.; and Peterson, Donald A.: Experimental Evaluation of 7.82-Inch (19.8-cm) Diameter Throat Inserts in a Storable-Propellant Rocket Engine. NASA TM X-1463, 1968.
8. Priem, Richard J.; and Heidemann, Marcus F.: Propellant Vaporization as a Design Criterion for Rocket-Engine Combustion Chambers. NASA TR R-67, 1960.
9. Gordon, Sanford; and McBride, Bonnie J.: Theoretical Performance of Liquid Hydrogen with Liquid Oxygen as a Rocket Propellant. NASA Memo 5-21-59E, 1959.
10. Pieper, Jerry L.: ICRPG Liquid Propellant Thrust Chamber Performance Evaluation Manual. CPIA Publ. 178, Johns Hopkins University (AD-843051), Sept. 30, 1968.
11. Back, L. H.; and Cuffel, R. F.: Flow Coefficients for Supersonic Nozzles with Comparatively Small Radius of Curvature Throats. J. Spacecraft Rockets, vol. 8, no. 2, Feb. 1971, pp. 196-198.

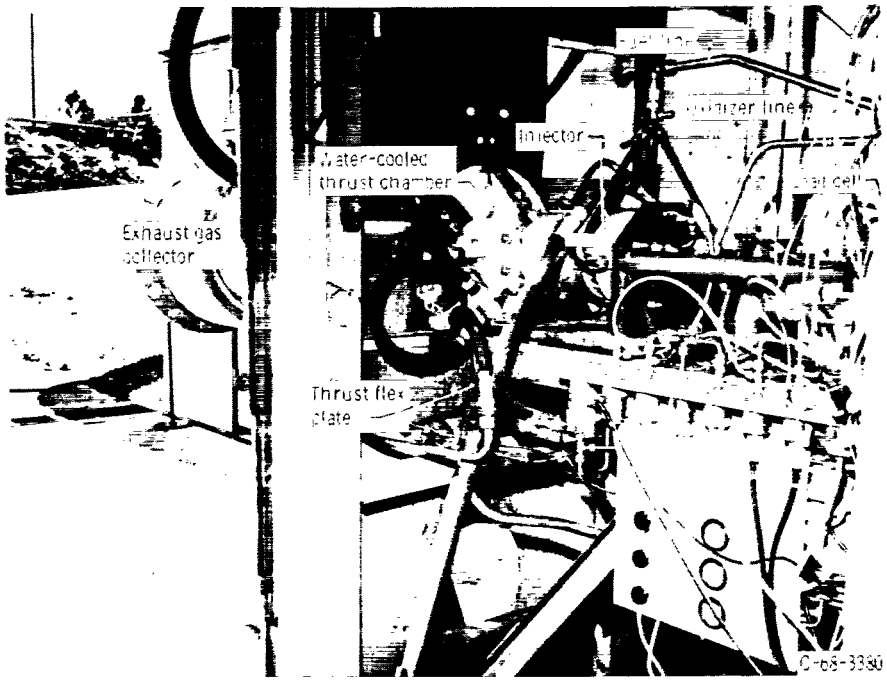

Figure 1. - Test facility.

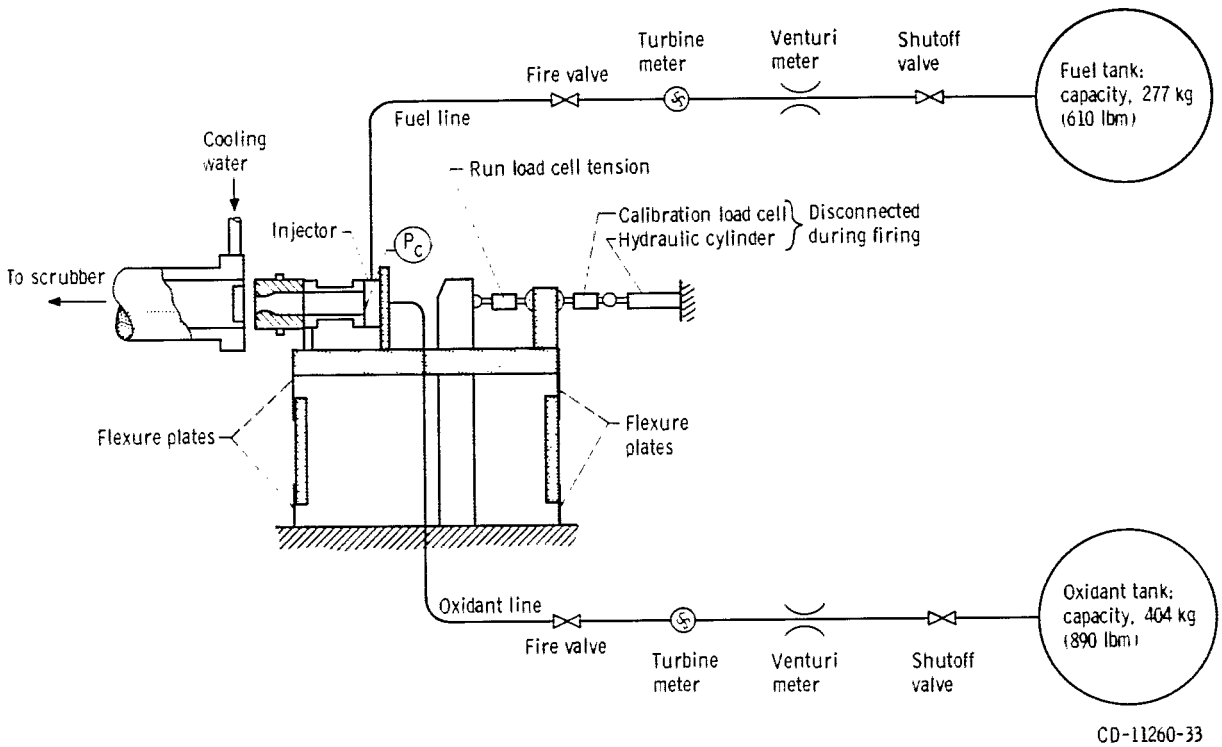

Figure 2. - Flow system.

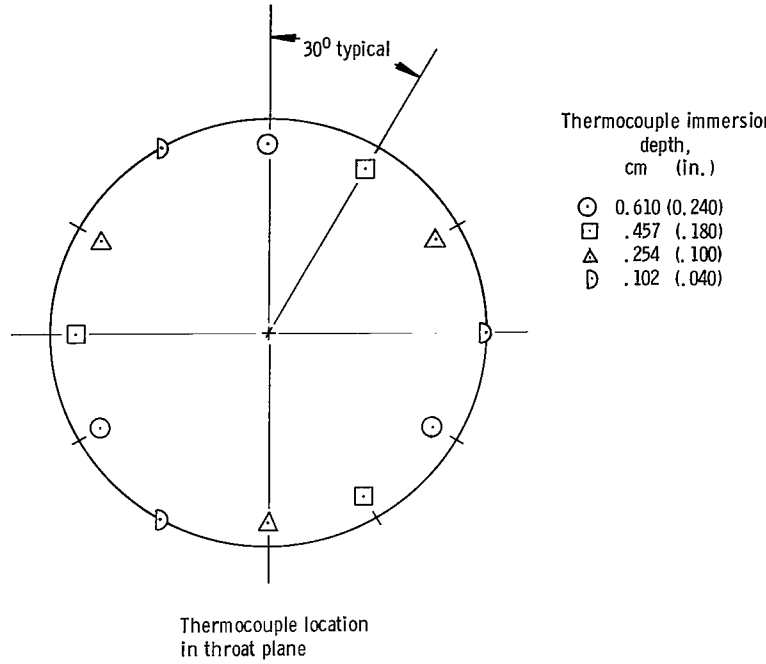

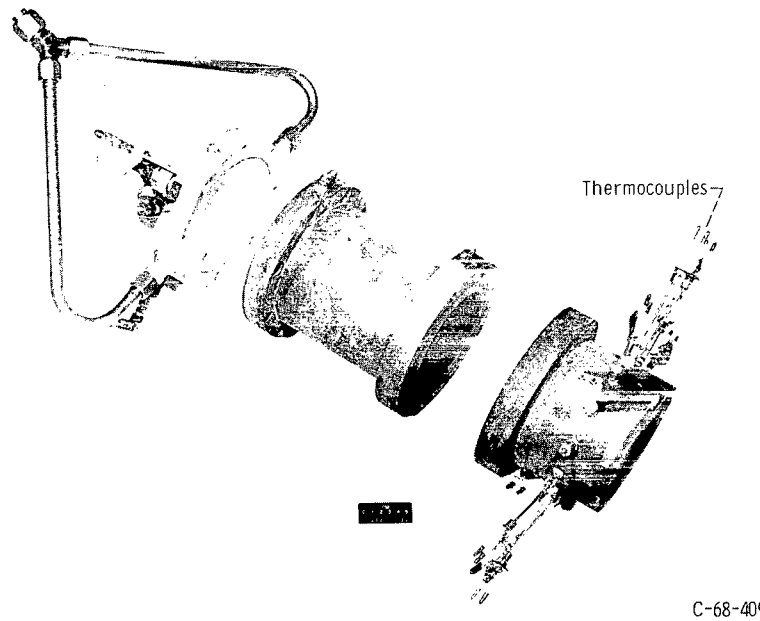

Figure 3. - Thrust chamber assembly: heat-sink chamber and nozzle. Thermocouple type, immersion.

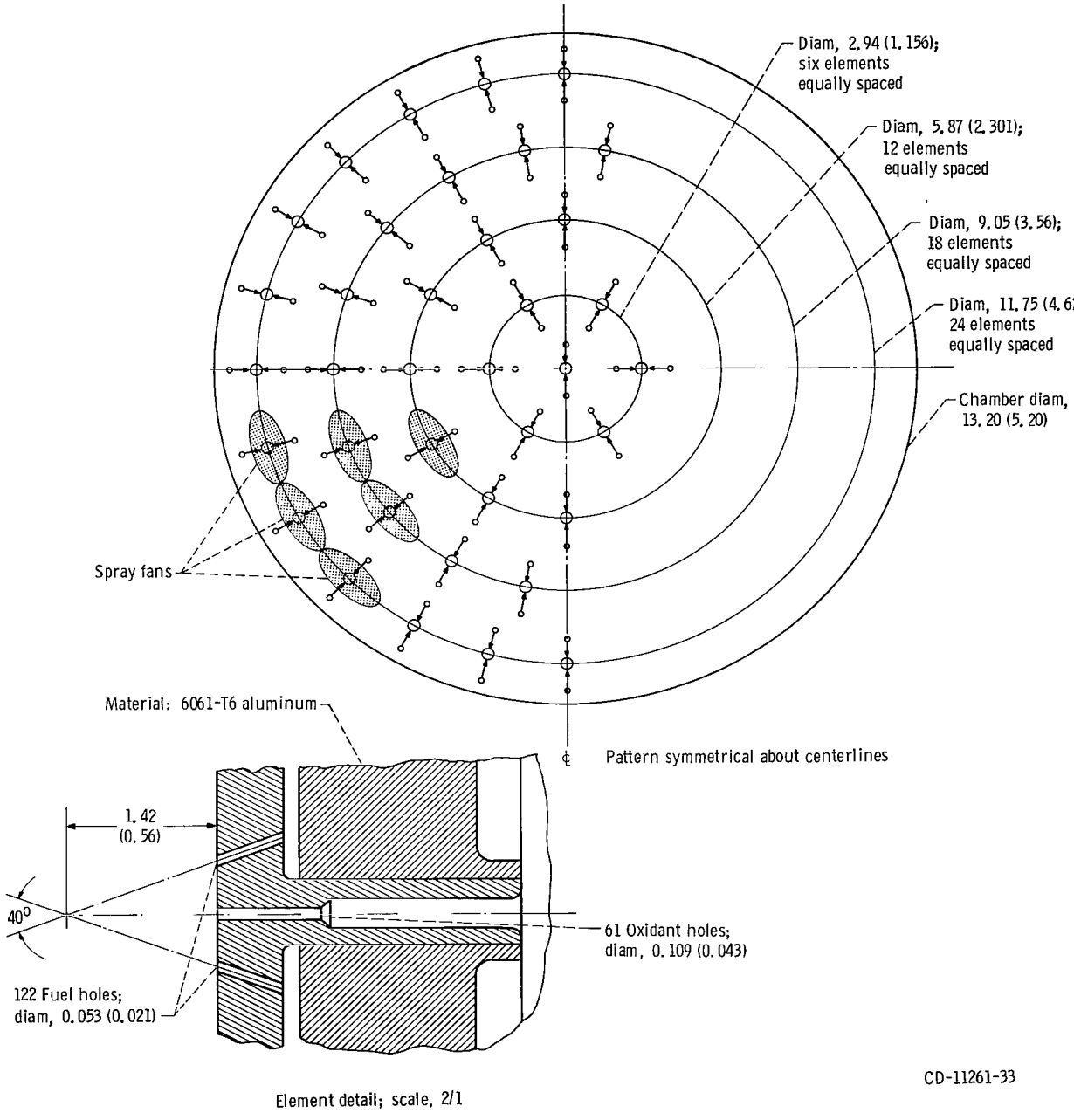

Figure 4. - Injector 1. (All dimensions not otherwise noted are in centimeters (in.).)

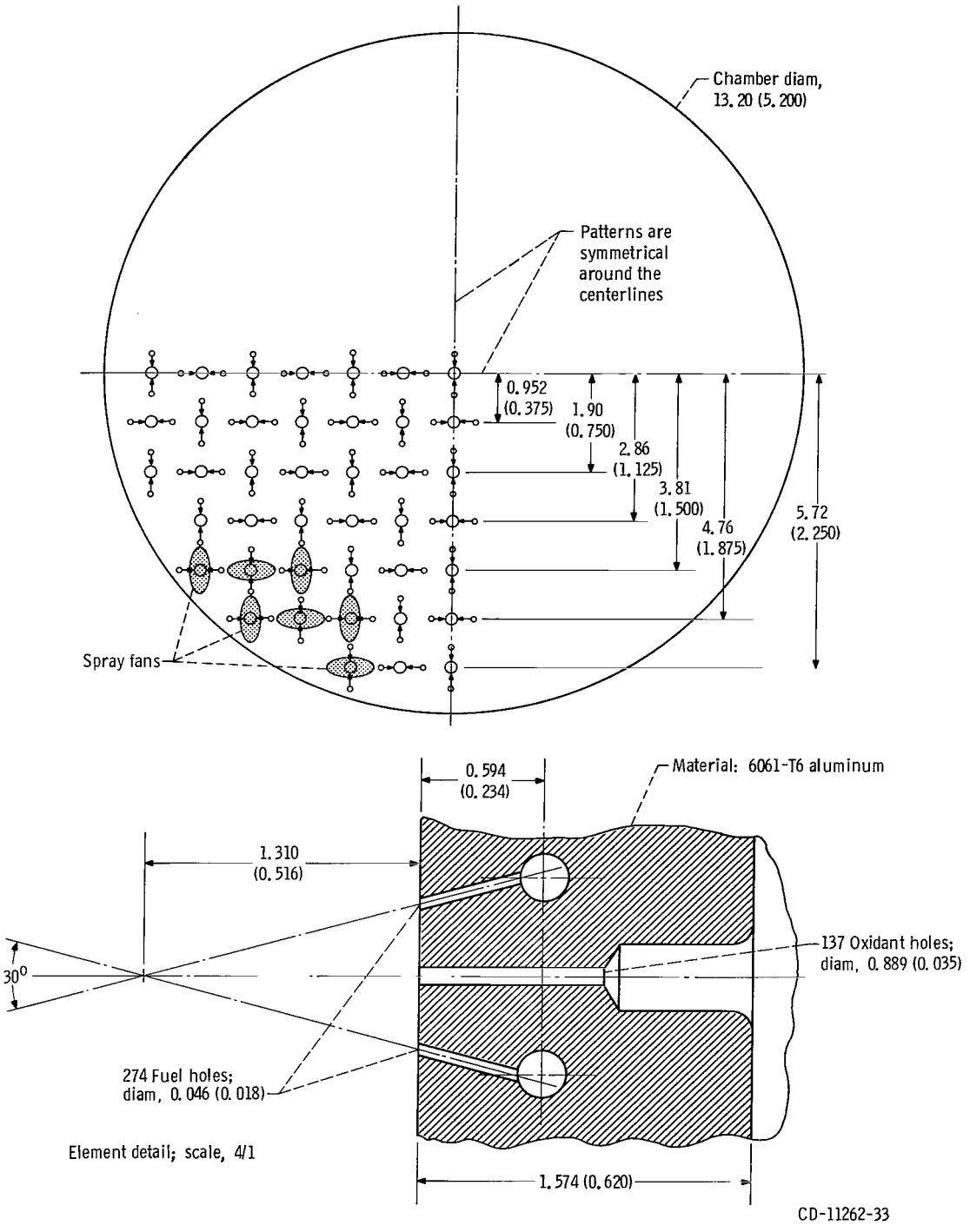

Figure 5. - Injector 2. (All dimensions not otherwise noted are in centimeters (in.).)

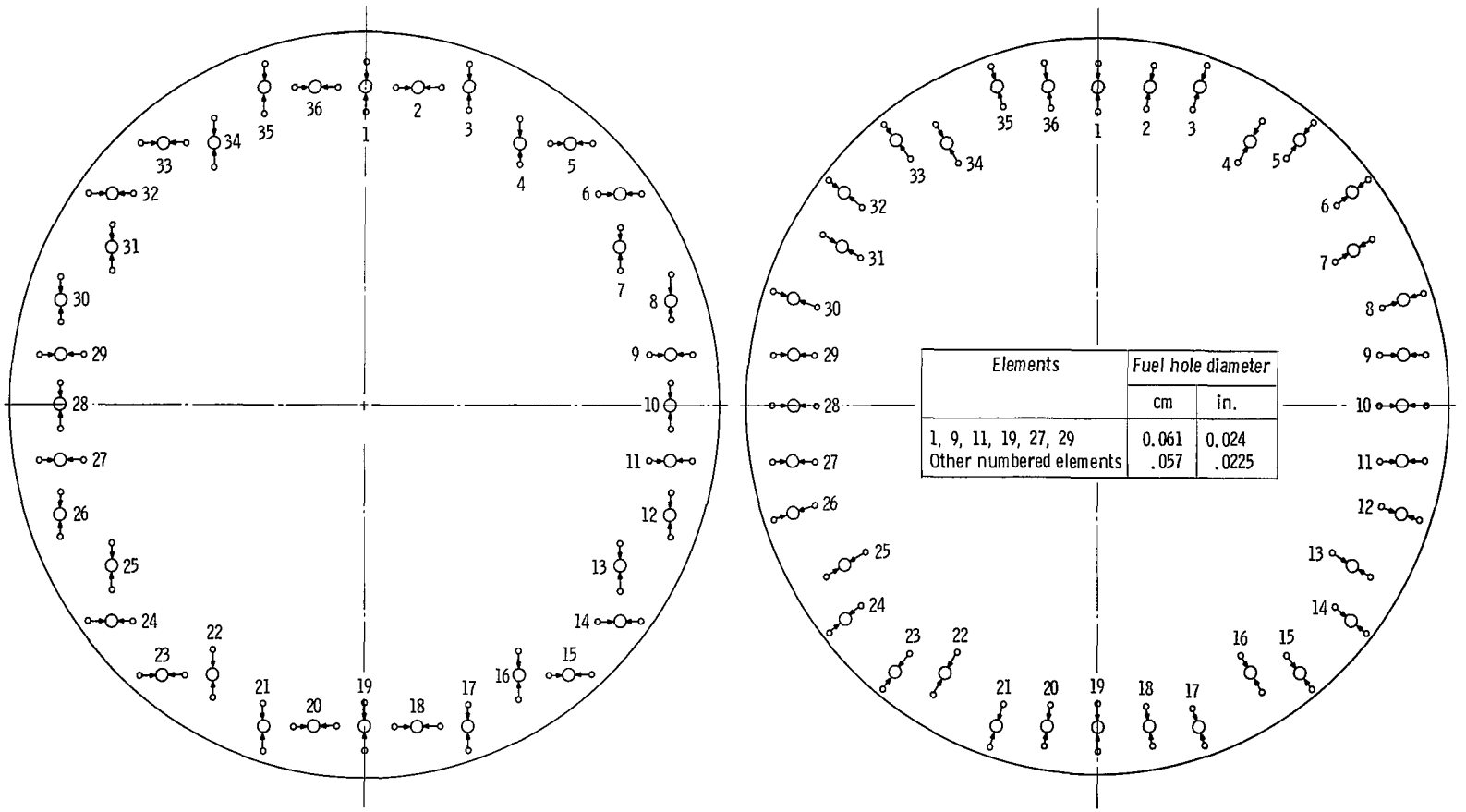

(a) Injector 2A. Fuel holes on elements 1 to 36 were enlarged to 0.061-centimeter (0.024-in.) diameter.

(b) Injector 2B.

CD-11263-33

Figure 6. - Modifications of injector 2. Chamber diameter, 13.20 centimeters (5.200 in.). All core elements in grid as in figure 5.

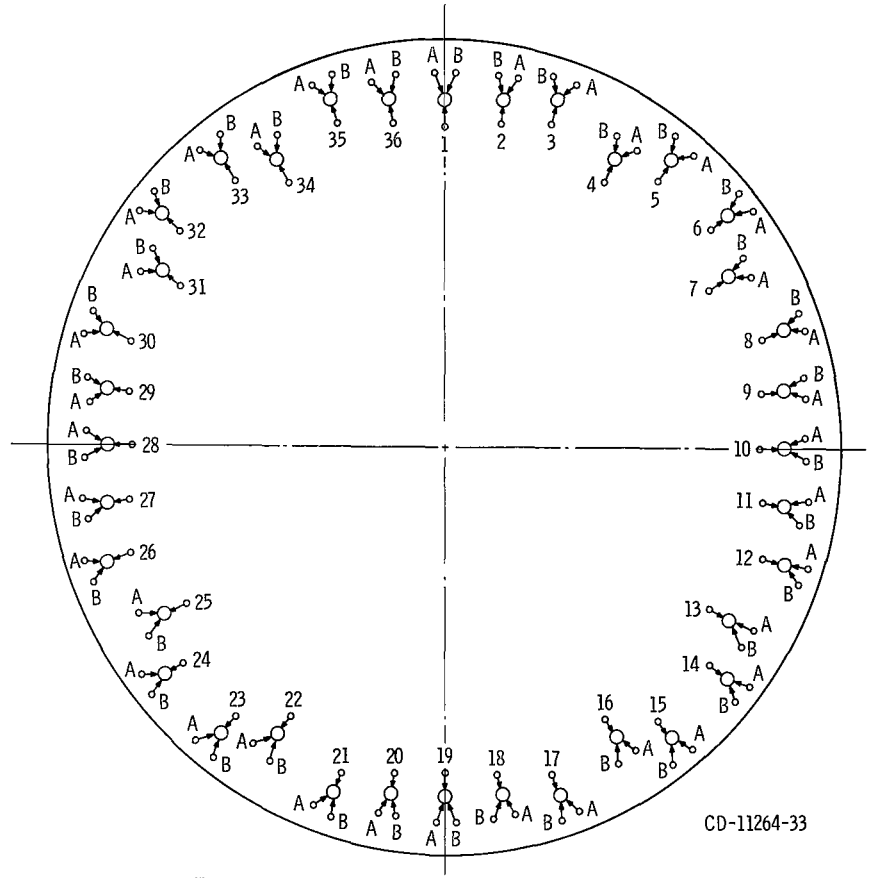

Elements	Fuel hole diameter			
	cm	in.	cm	in.
	Outside (two)		Inside (one)	
3, 17, 21, 35	0.061	0.024	0.057	0.0225
1, 9, 11, 19, 27, 29	.041	.016	.061	.024
All other numbered elements	.041	.016	.057	.0225

(c) Injector 2C.

Figure 6. - Continued.

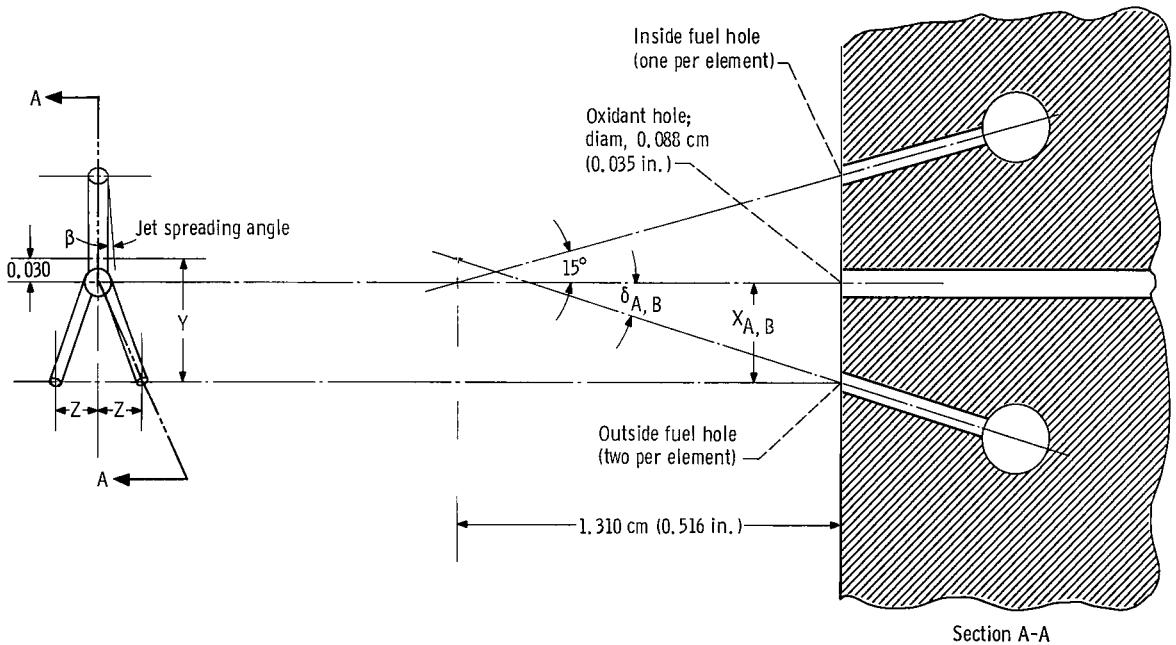

CD-11265-33

A AND B NOTATION ON FIG. 6(c)

Element	Y_A		Z_A		Y_B		Z_B		X_A		δ_A	X_B		δ_B
	cm	in.	cm	in.	cm	in.	cm	in.	cm	in.		cm	in.	
10, 28	0.401	0.1576	0.148	0.0585	0.401	0.1576	0.148	0.0585	0.434	0.1710	18° 20'	0.434	0.1710	18° 20'
9, 11, 27, 29	.401	.1576	.148	.0585	.401	.1576	.148	.0585	.434	.1710	18° 20'	.434	.1710	18° 20'
8, 12, 26, 30	.373	.1470	.138	.0545	.478	.1884	.177	.0696	.405	.1595	17° 10'	.517	.2035	21° 30'
7, 13, 25, 31	.376	.1479	.139	.0549	.455	.1790	.168	.0662	.408	.1605	17° 20'	.492	.1935	20° 30'
6, 14, 24, 32	.385	.1515	.143	.0563	.416	.1638	.155	.0610	.418	.1645	17° 40'	.454	.1785	19° 0'
5, 15, 23, 33	.416	.1638	.155	.0610	.385	.1515	.143	.0563	.454	.1785	19° 0'	.418	.1645	17° 40'
4, 16, 22, 34	.455	.1790	.168	.0662	.376	.1419	.139	.0549	.492	.1935	20° 30'	.408	.1605	17° 20'
3, 17, 21, 35	.422	.1663	.154	.0605	Existing		Existing		.450	.1770	19° 0'	.352	.1385	15° 0'
2, 18, 20, 36	.433	.1705	.160	.0631	.381	.1502	.142	.0558	.469	.1845	19° 40'	.414	.1630	17° 30'
1, 19	.401	.1576	.148	.0585	.401	.1576	.148	.0585	.434	.1710	18° 20'	.434	.1710	18° 20'

(d) Element d_6

Figure 6. - Concluded.

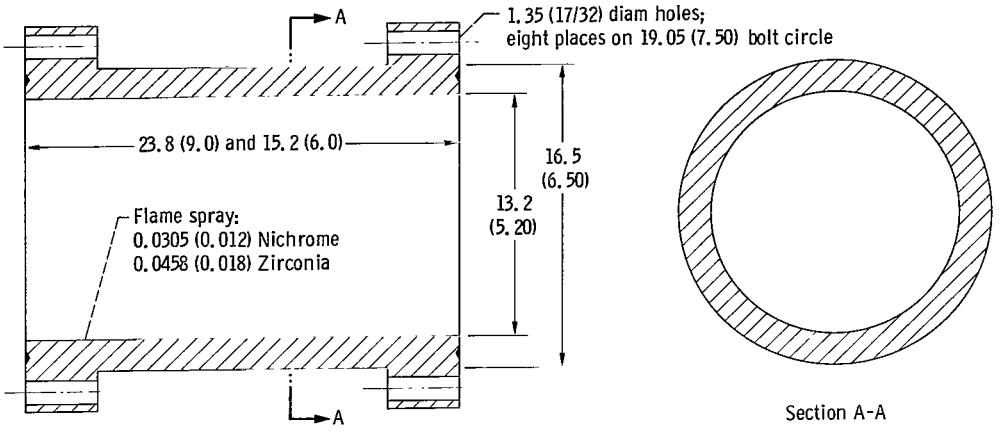

(a) Chamber; diameter, 13.2 centimeters (5.20 in.).

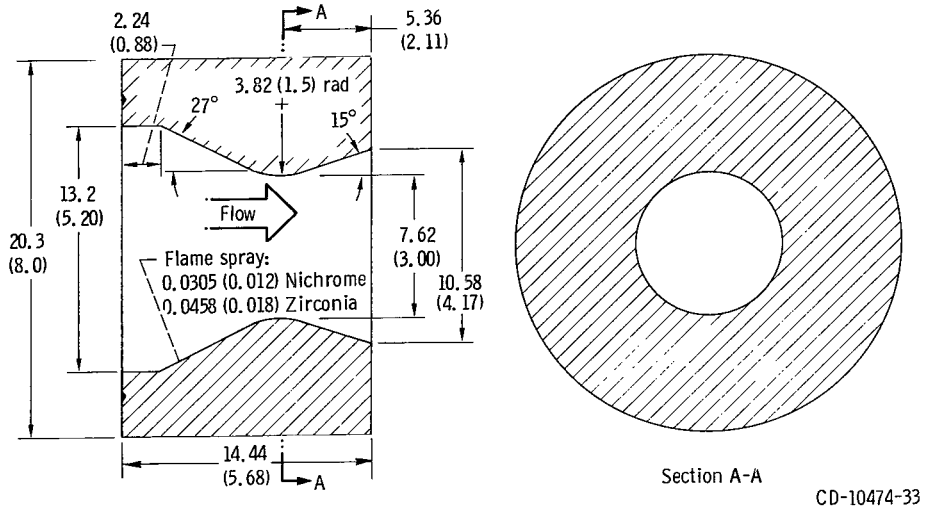

(b) Nozzle; throat diameter, 7.62 centimeters (3.0 in.).

Figure 7. - Heat-sink thrust chamber. Material, mild steel. (All linear dimensions are in centimeters (in.).)

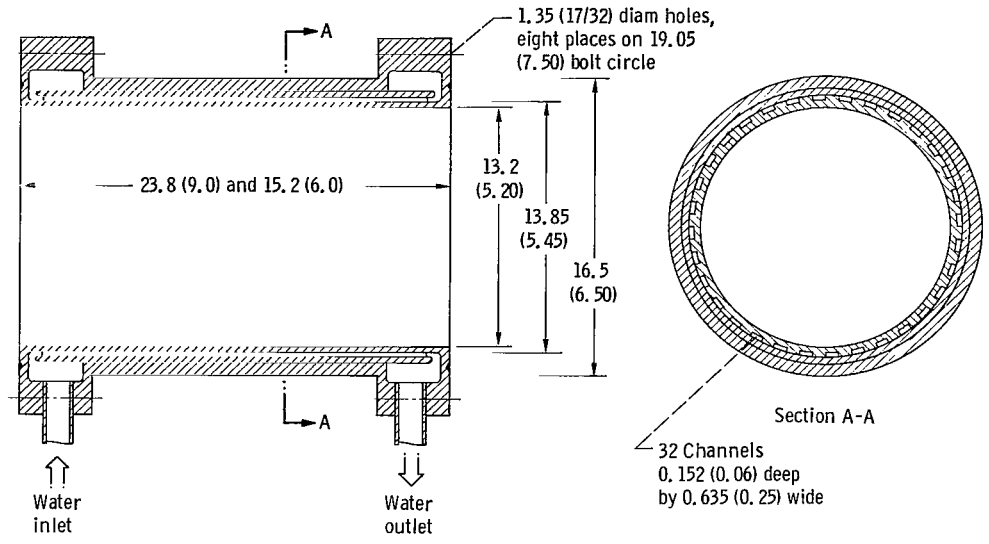

(a) Chamber; diameter, 13.2 centimeters (5.20 in.).

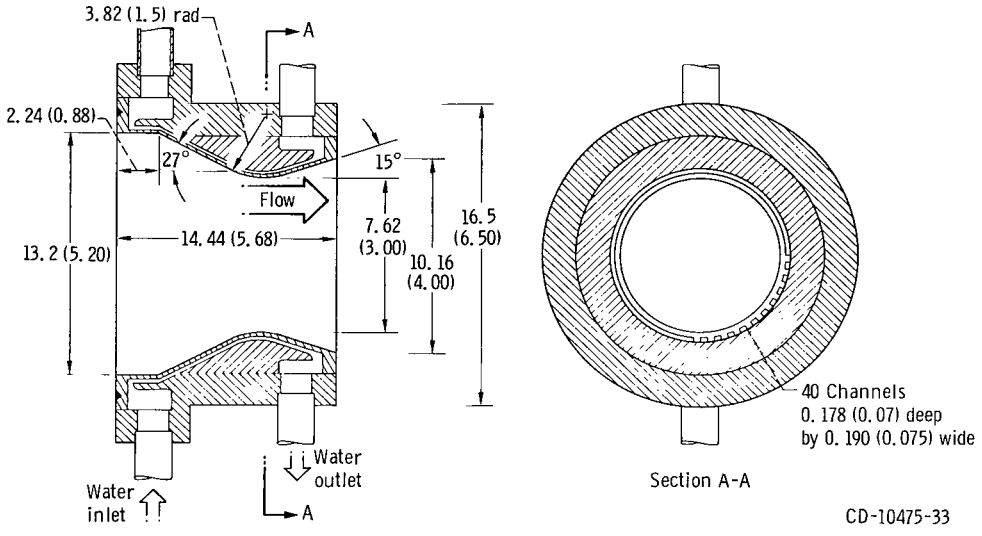

(b) Nozzle; throat diameter, 7.62 centimeters (3.0 in.)

Figure 8. - Water-cooled thrust chamber. Material, 6061-T6 aluminum. (All linear dimensions are in centimeters (in.).)

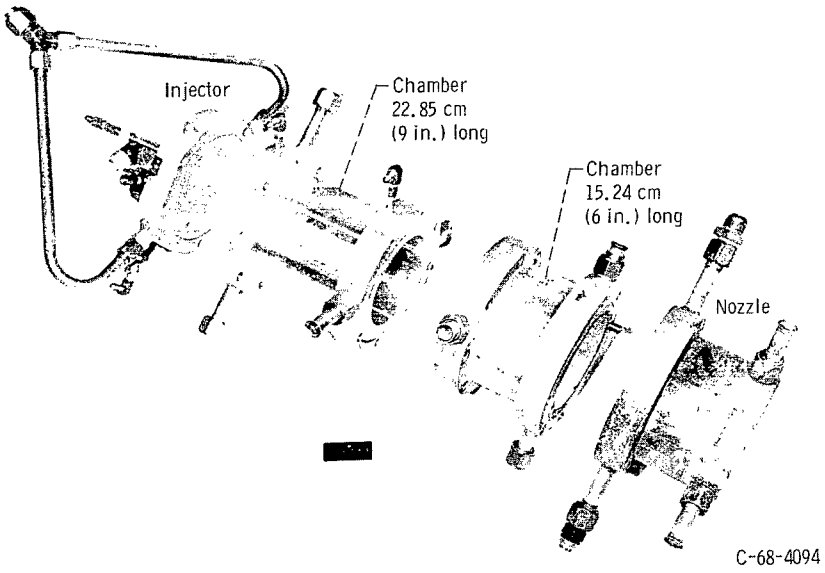

Figure 9. - Thrust chamber assembly: water-cooled chamber and nozzle.

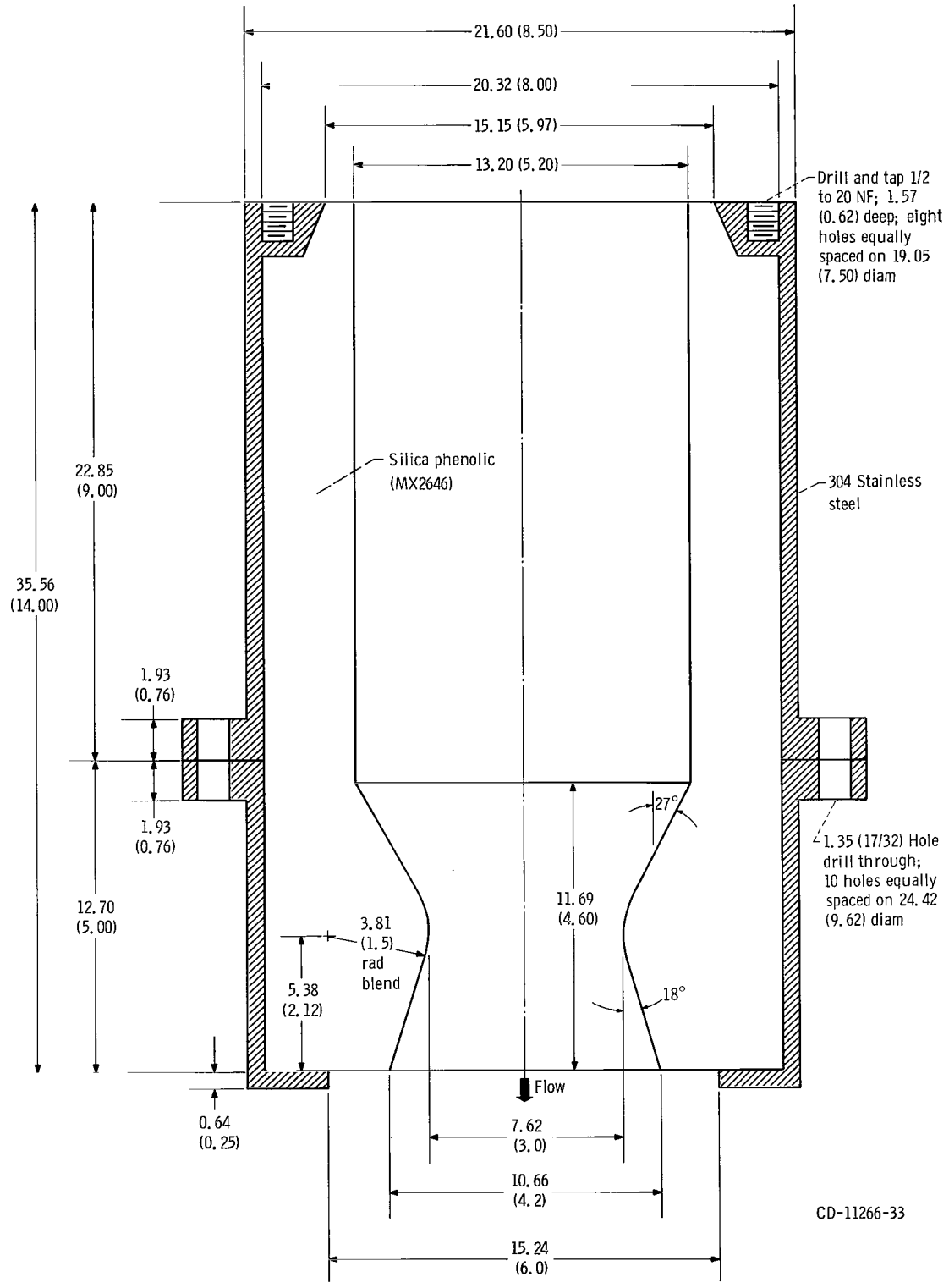

Figure 10. - Ablative thrust chamber. (All linear dimensions are in centimeters (in.).)

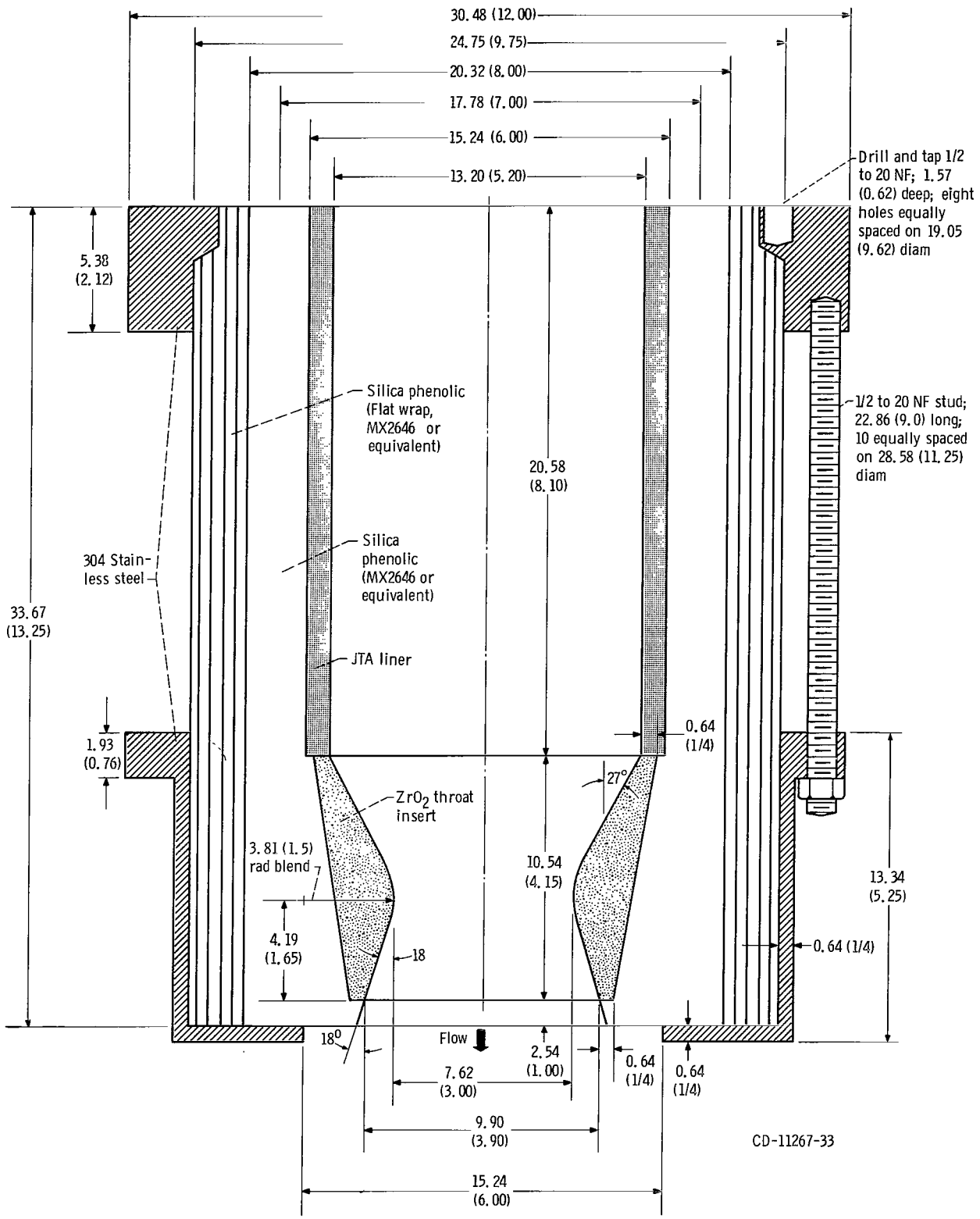

Figure 11. - Ablative thrust chamber with liner and throat insert. (All linear dimensions are in centimeters (in.).)

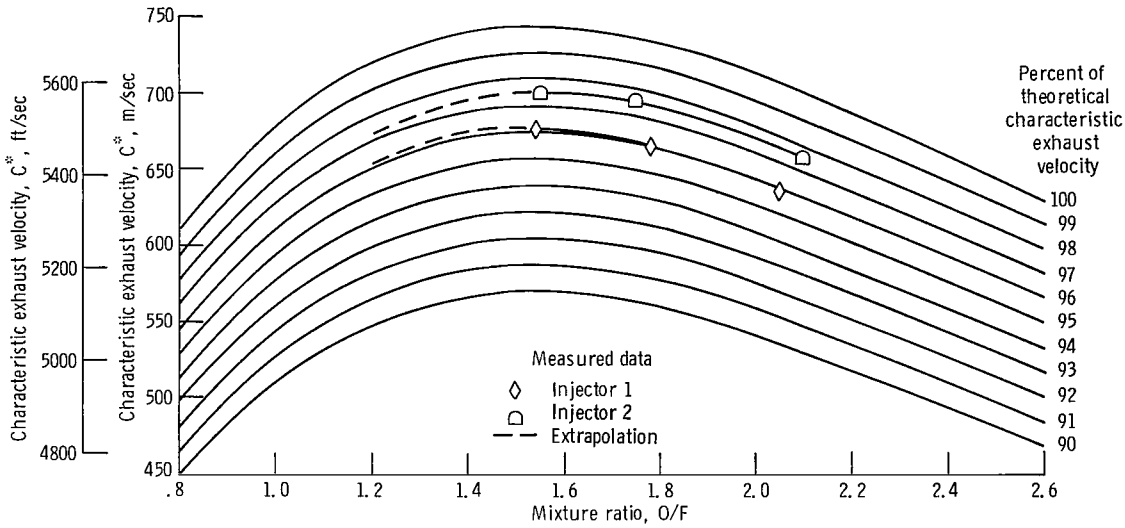

Figure 12. - Performance of original injector.

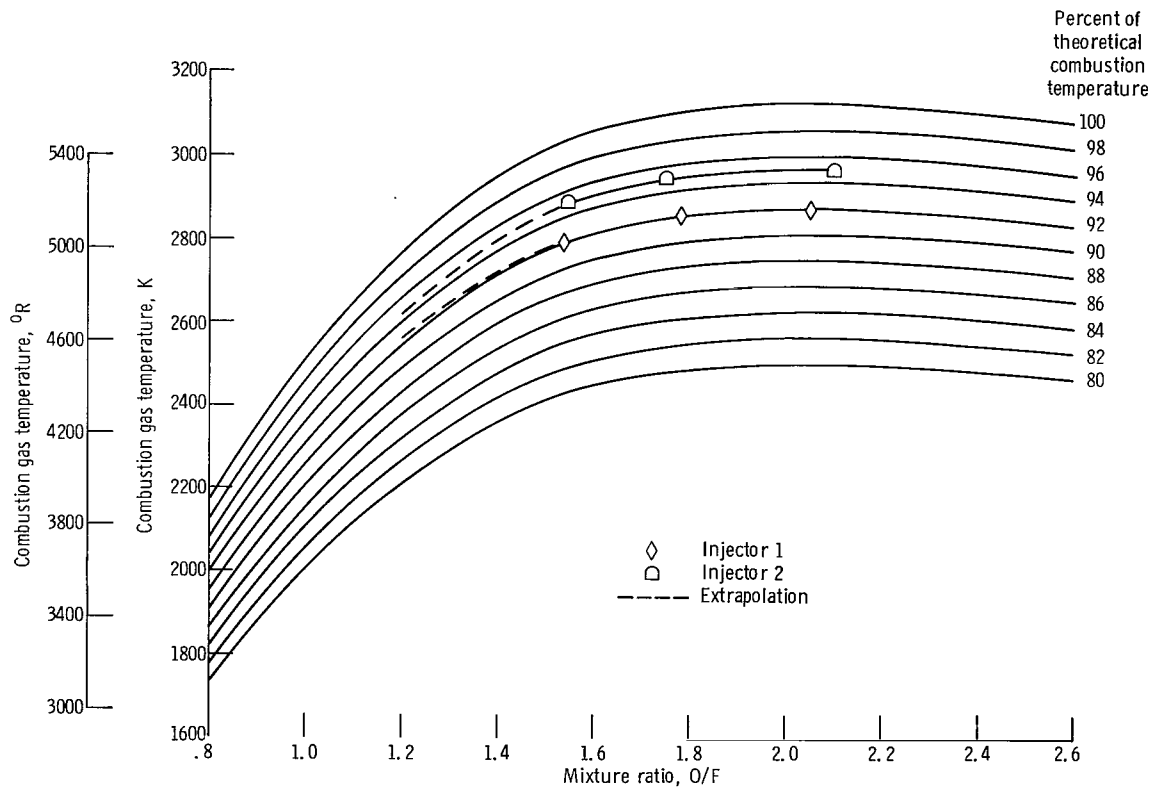

Figure 13. - Calculated combustion temperature - injectors 1 and 2.

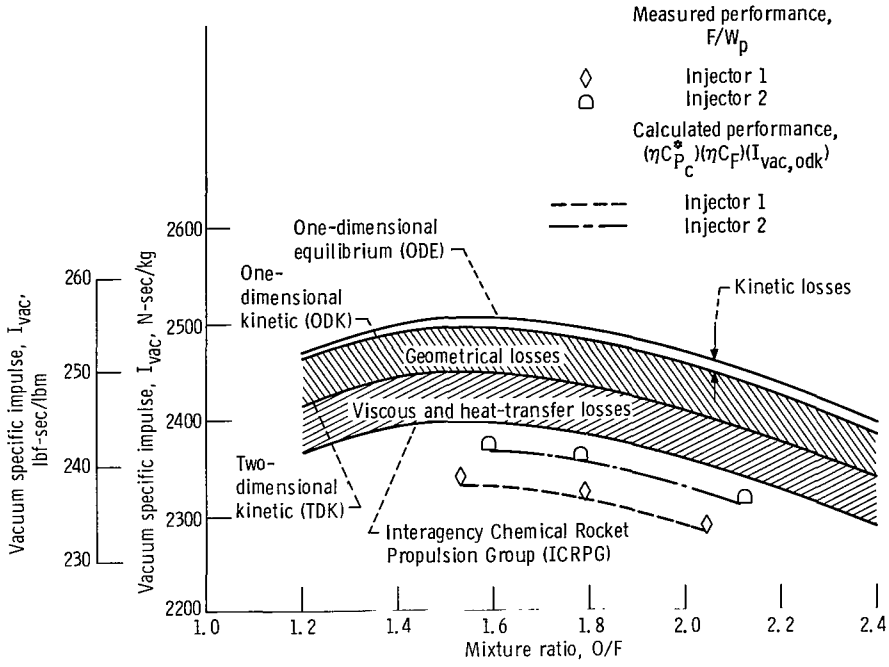

Figure 14. - Measured engine performance. Expansion area ratio, 1.80; conical nozzle (divergence half-angle, 15^0).

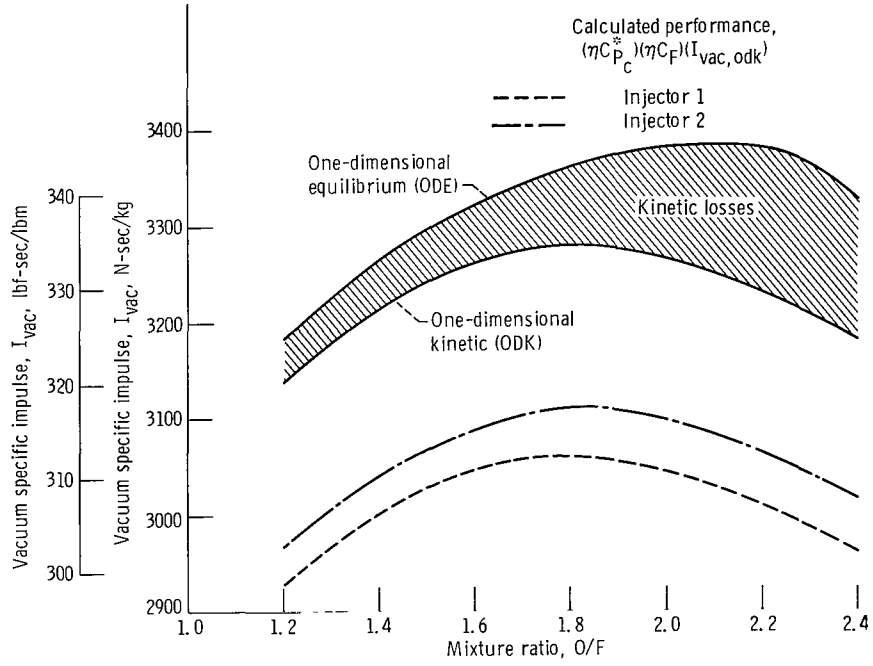

Figure 15. - Calculated engine performance. Expansion area ratio, 60; conical nozzle (divergence half-angle, 15^0).

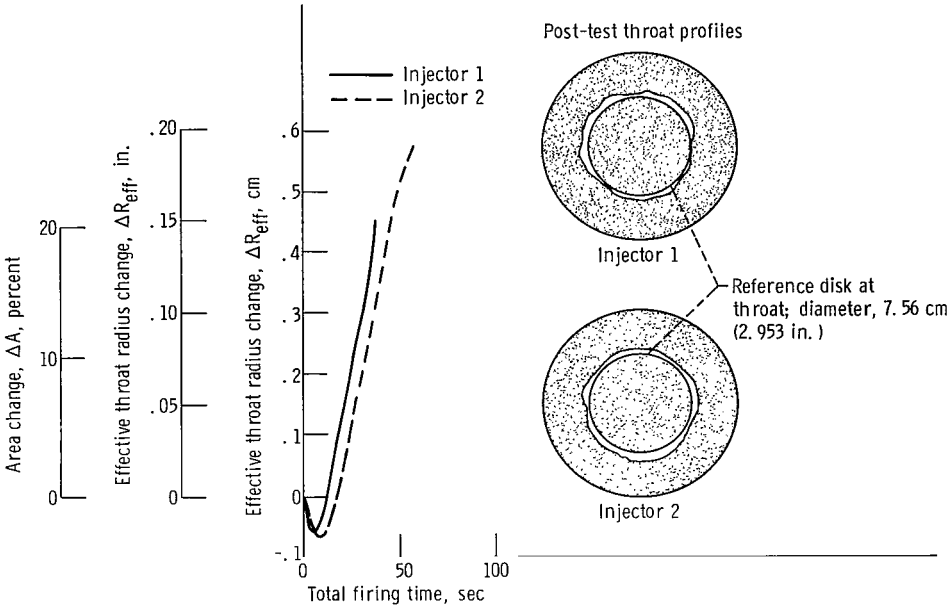

Figure 16. - Ablative throat erosion comparison - injectors 1 and 2.

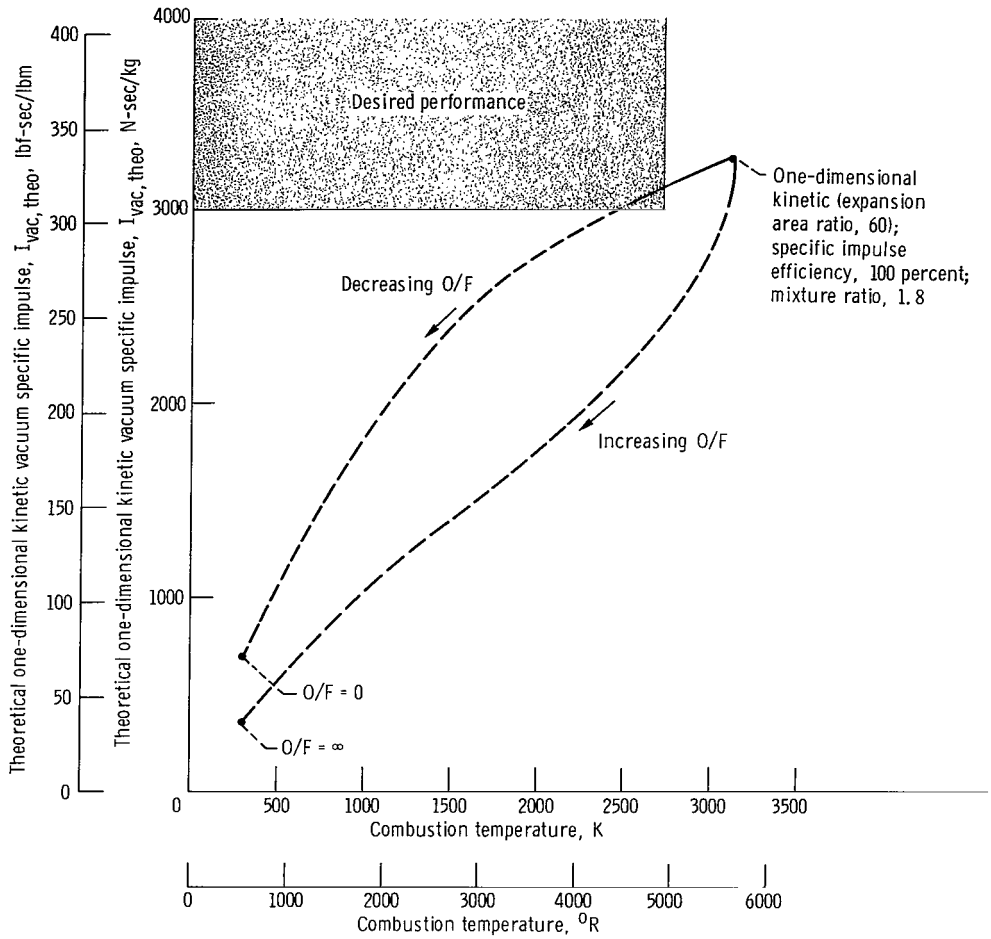

Figure 17. - Effect of mixture ratio (O/F) variation on combustion temperature and performance.

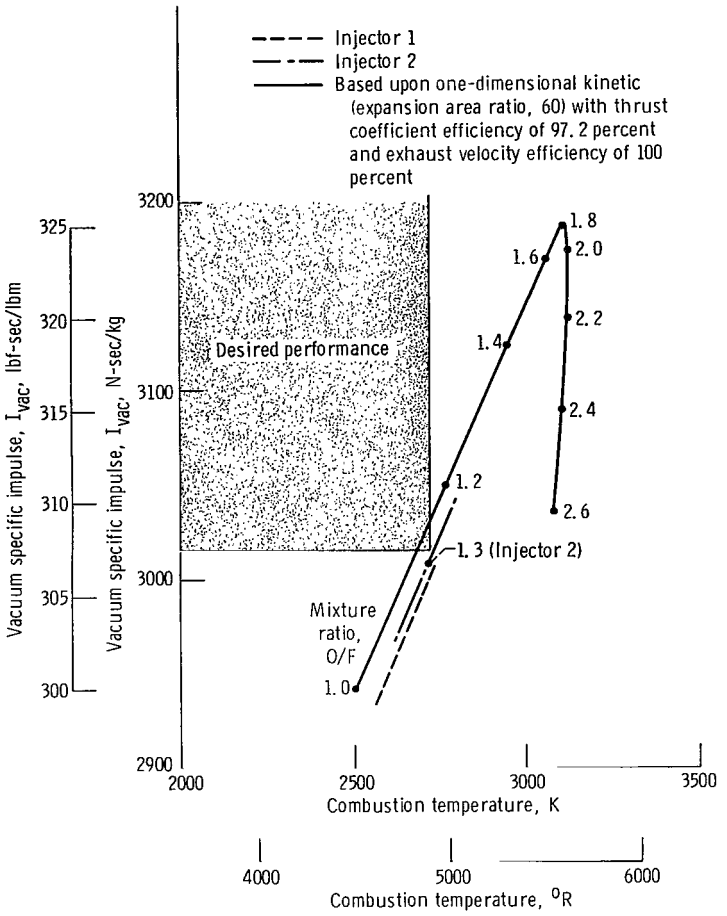

Figure 18. - Effect of mixture ratio (O/F) variation on combustion temperature and performance.

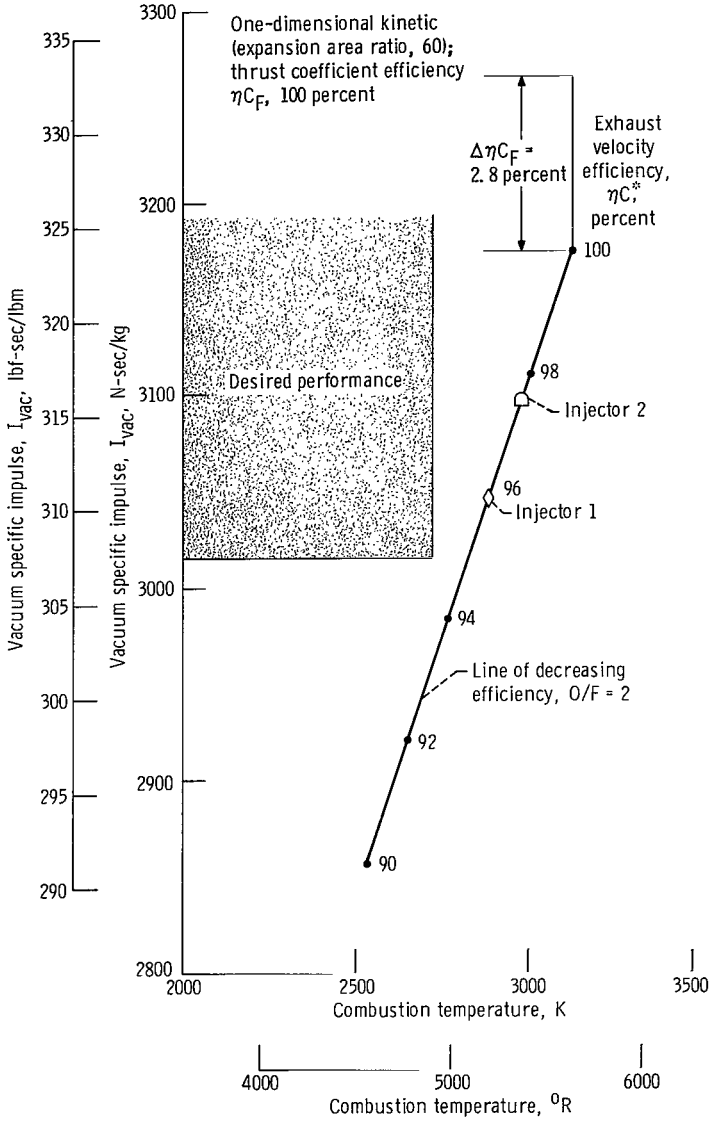

Figure 19. - Effect of efficiency on combustion temperature and performance. Mixture ratio, 2.0.

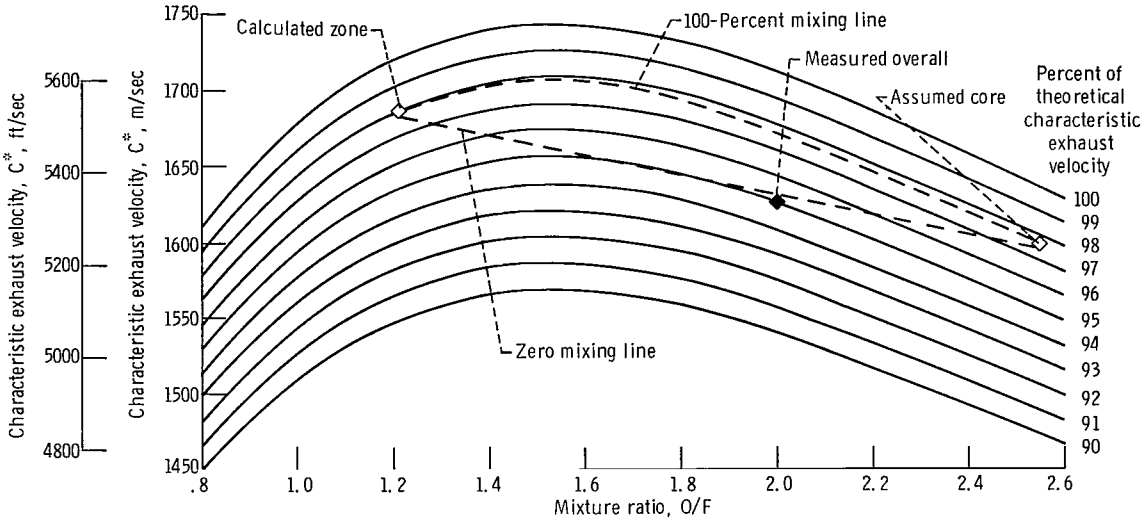

Figure 20. - Zoned injector performance - injector 2A.

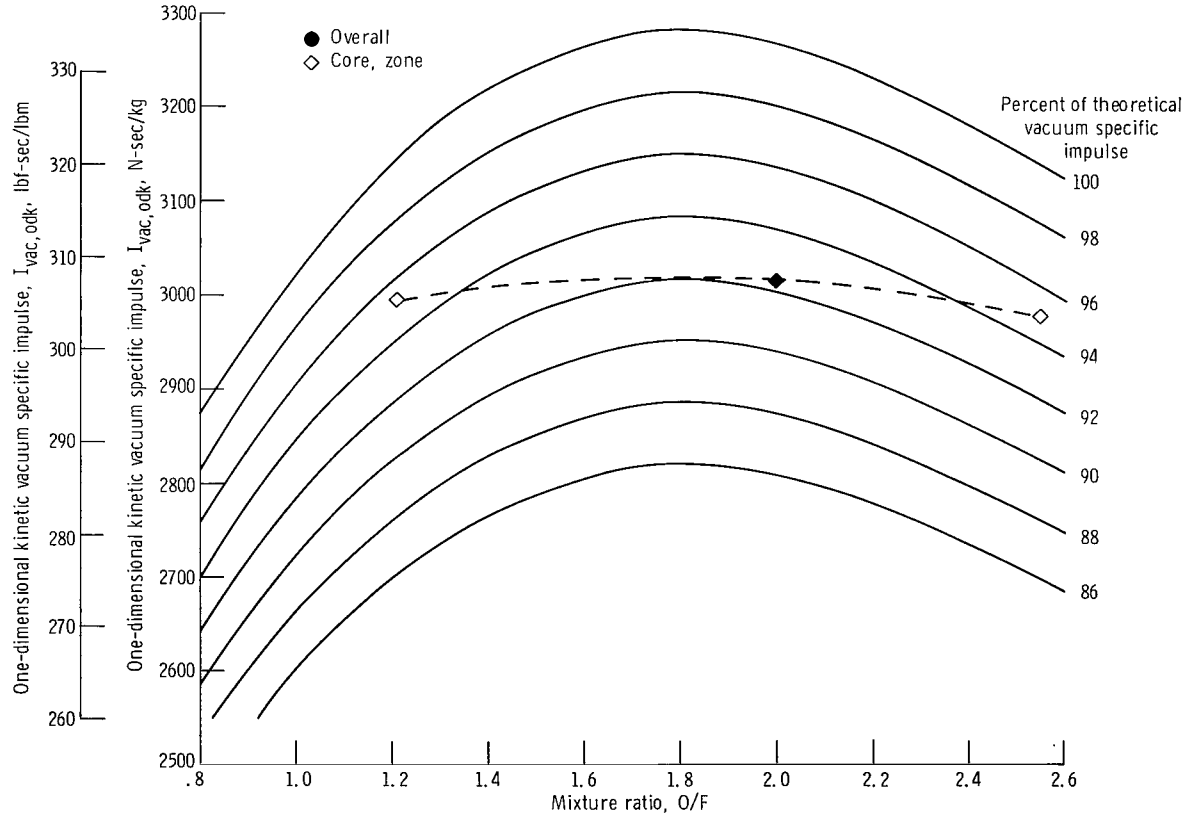

Figure 21. - Calculated engine performance - injector 2A. Nozzle expansion area ratio, 60; conical nozzle (divergence half-angle, 15^0).

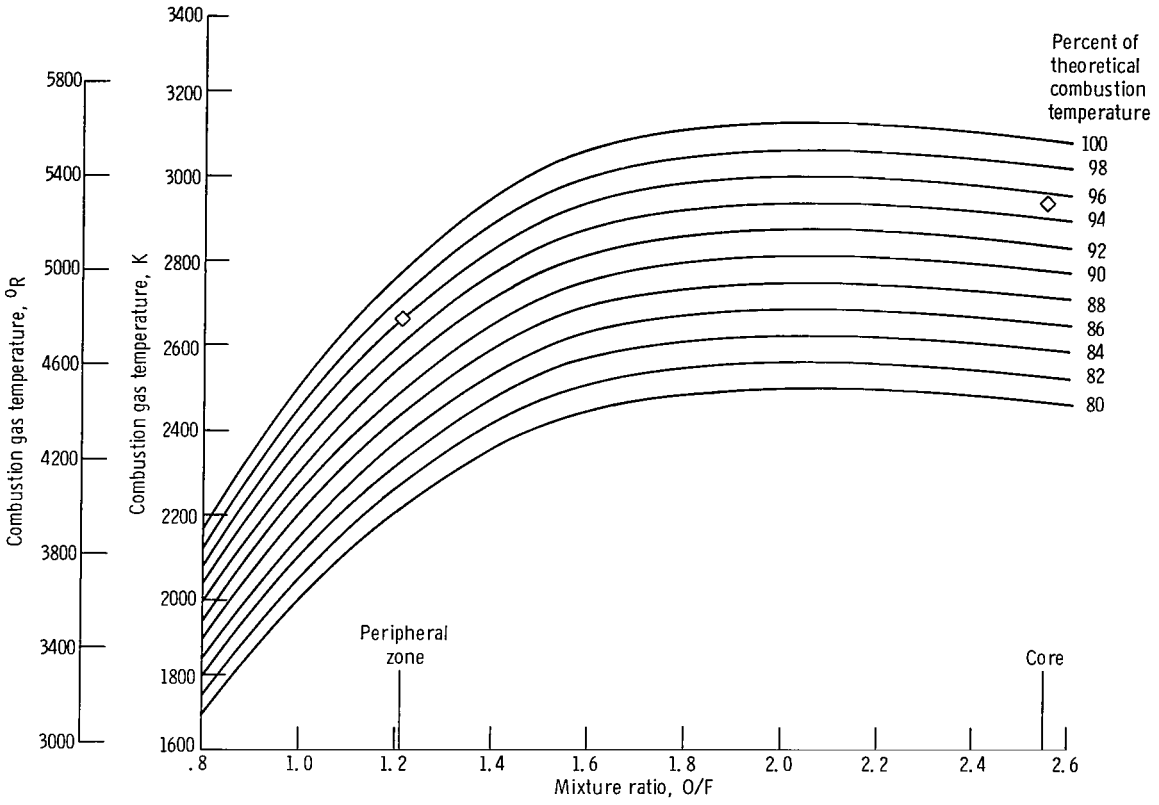

Figure 22. - Calculated combustion temperature - injector 2A.

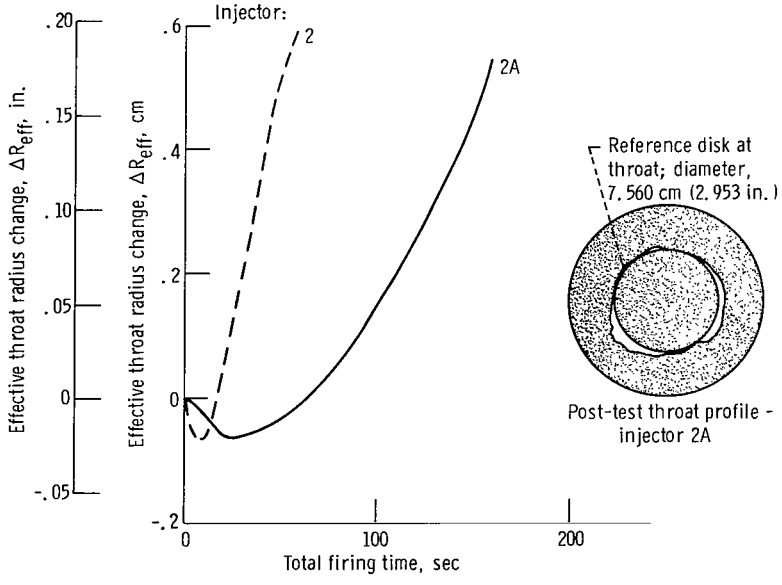

Figure 23. - Ablative throat erosion comparison - injectors 2 and 2A.

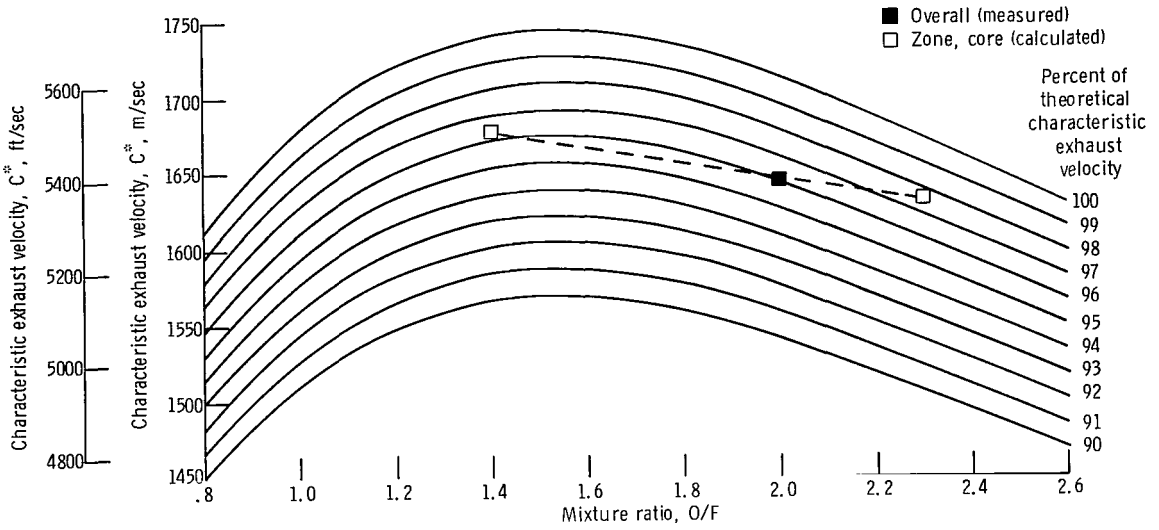

Figure 24. - Zoned injector performance - injector 2B.

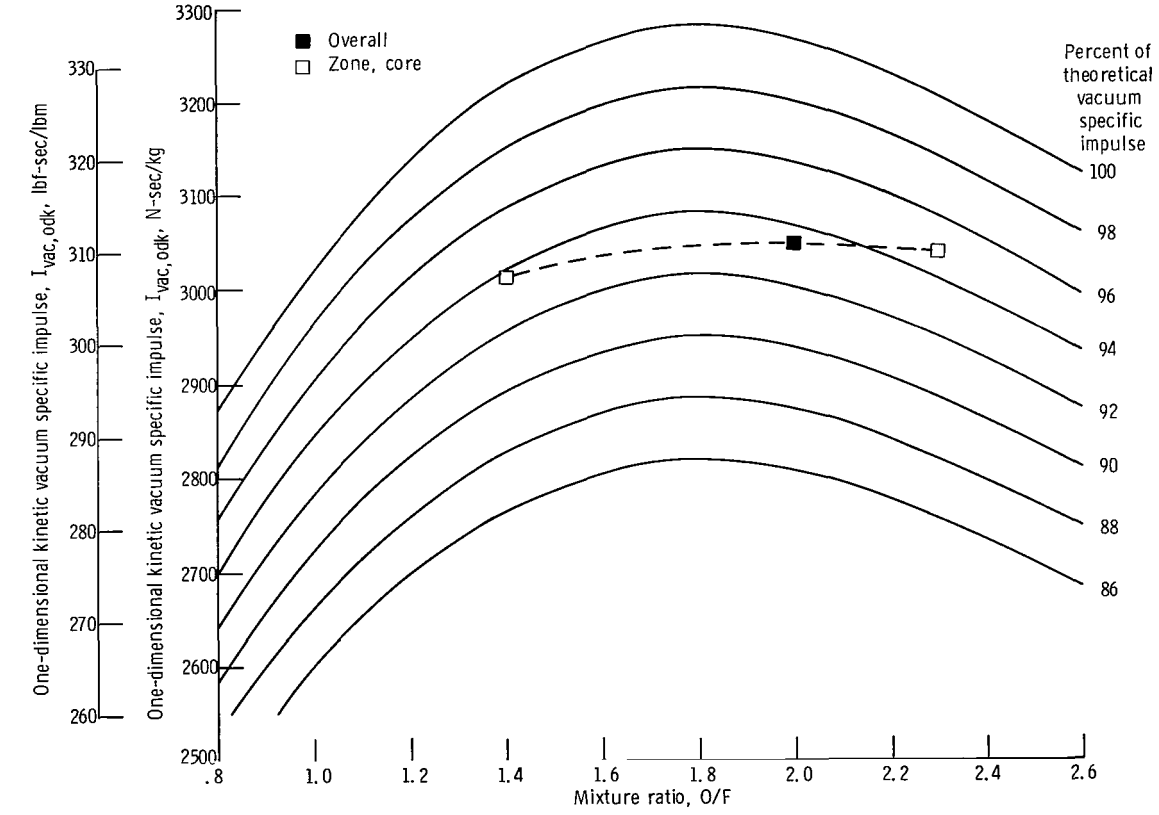

Figure 25. - Calculated engine performance - injector 2B. Nozzle expansion area ratio, 60; conical nozzle (divergence half-angle, 15^0).

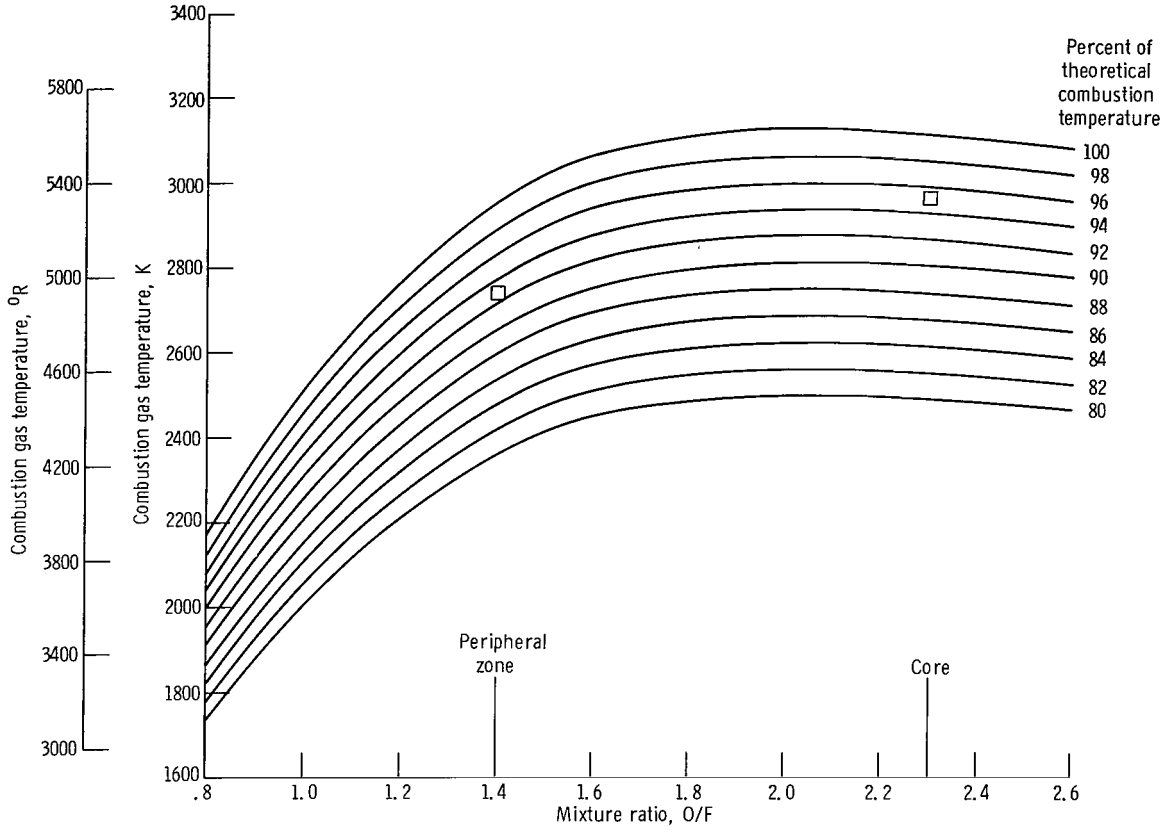

Figure 26. - Calculated combustion temperature - injector 2B.

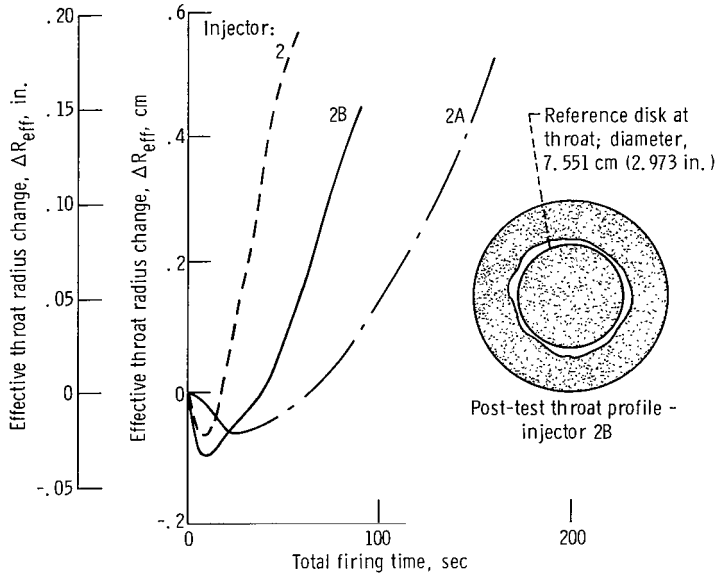

Figure 27. - Ablative throat erosion comparison - injectors 2, 2A, and 2B.

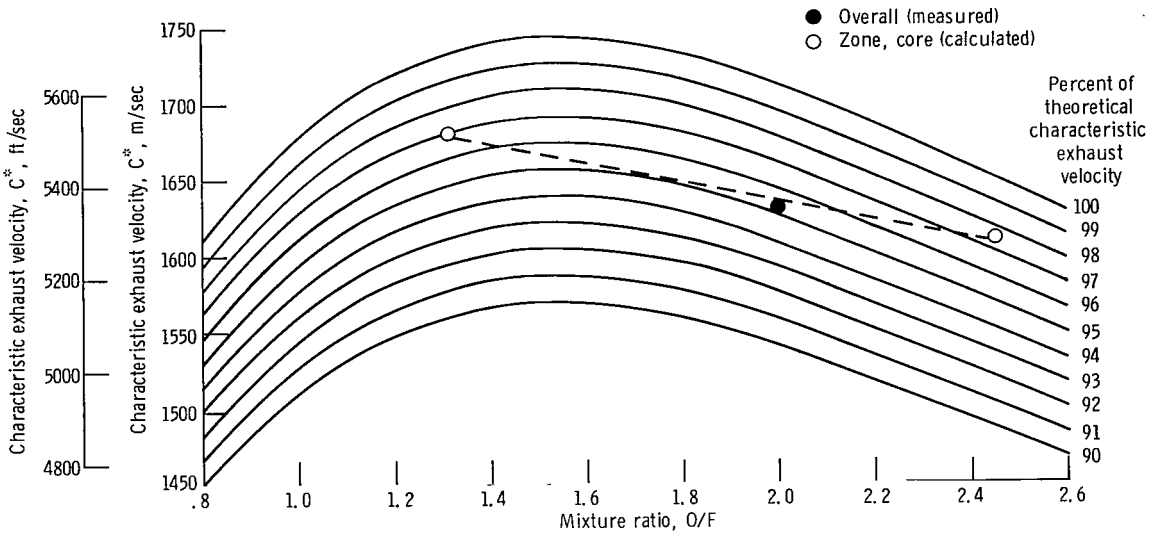

Figure 28. - Zoned injector performance - injector 2C.

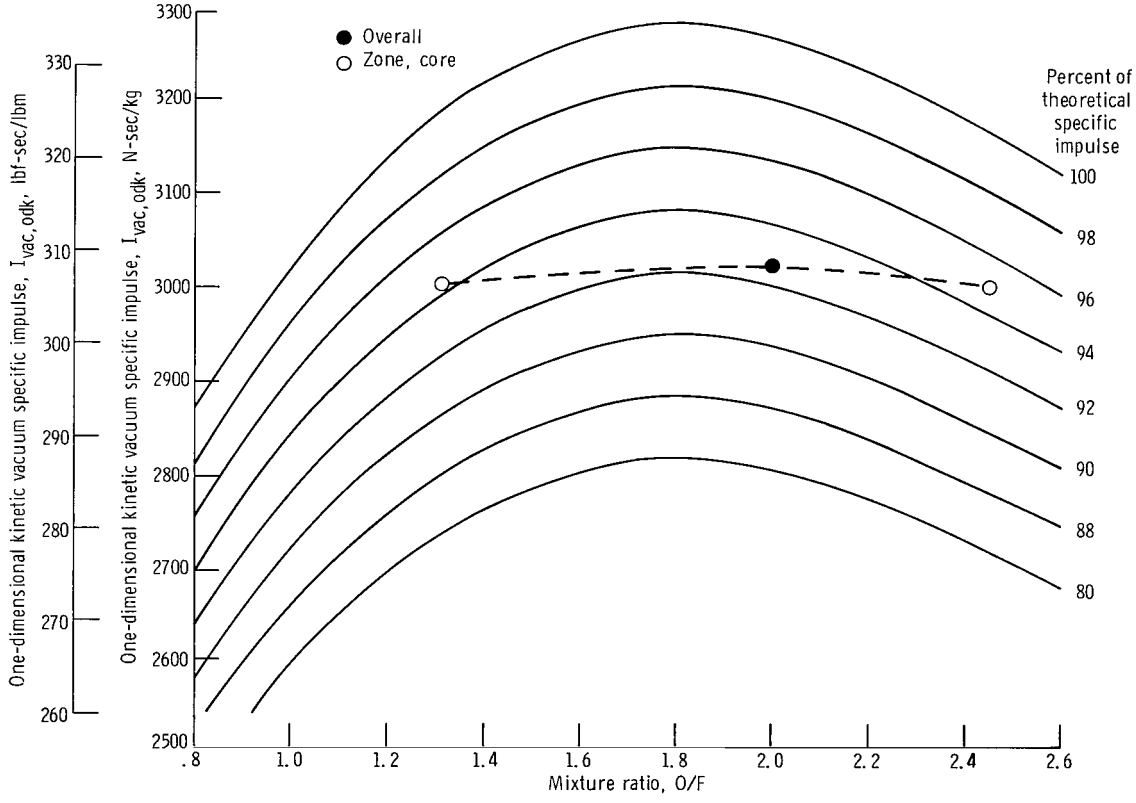

Figure 29. - Calculated engine performance - injector 2C. Nozzle expansion area ratio, 60; conical nozzle (divergence half-angle, 15^0).

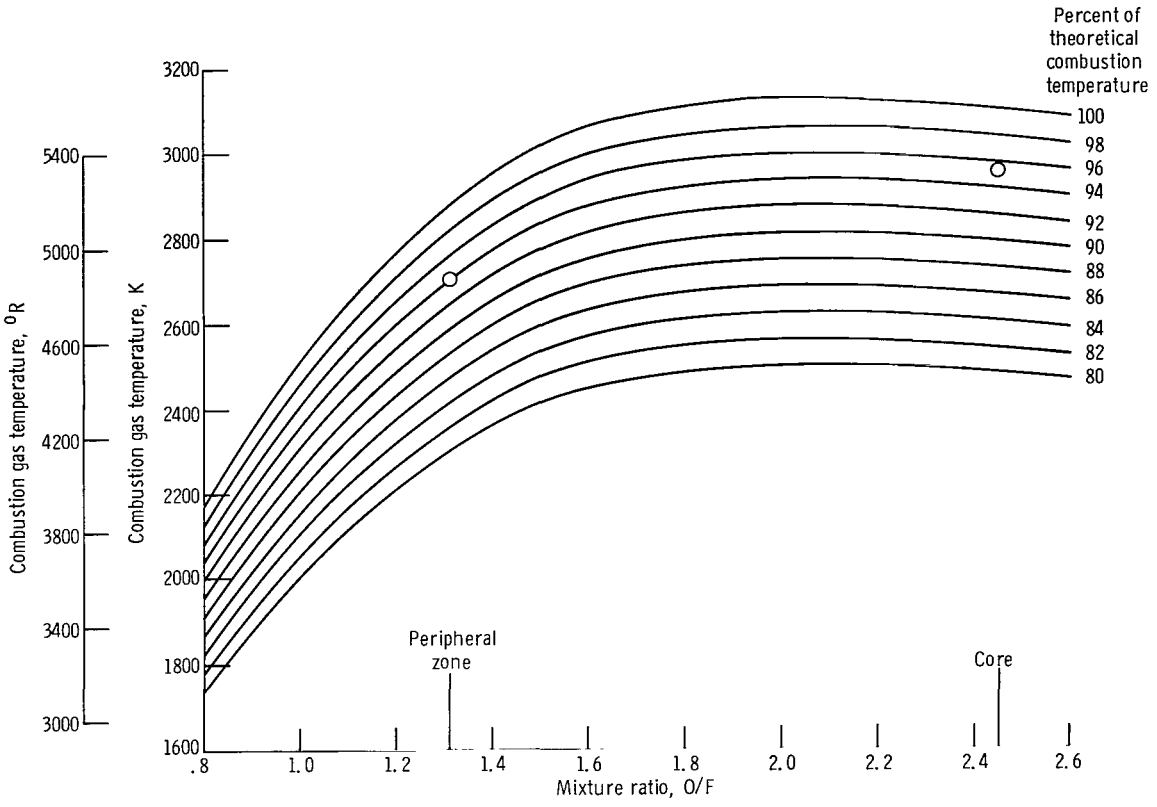

Figure 30. - Calculated combustion temperature - injector 2C.

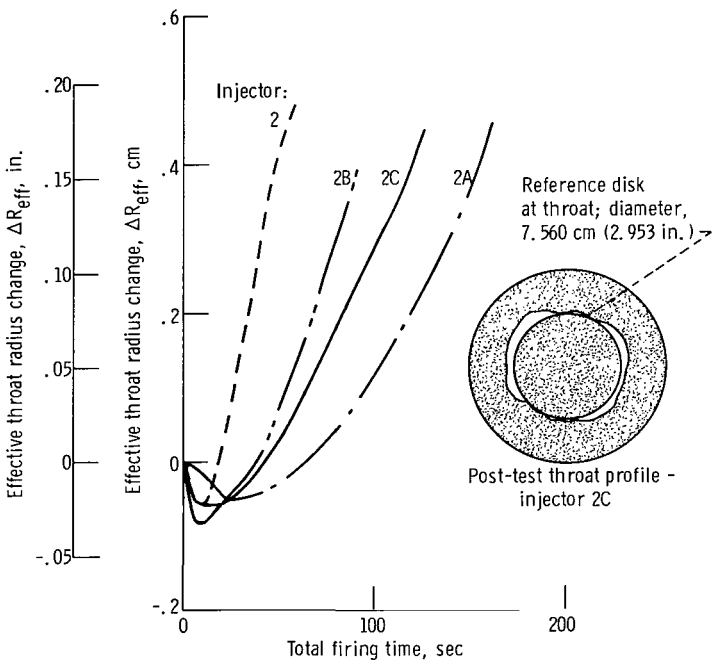

Figure 31. - Ablative throat erosion comparison - injectors 2, 2A, 2B, and 2C.

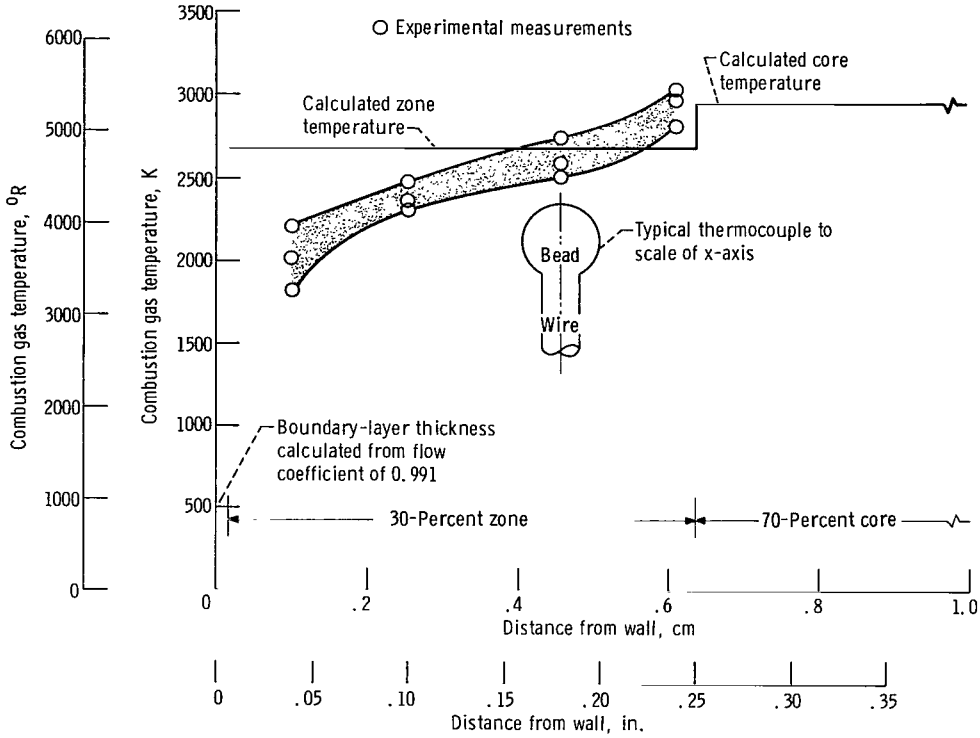

Figure 32. - Measured combustion temperature profile at wall in throat plane - injector 2C. Chamber pressure, 690 kN m^2 (100 psia); overall mixture ratio, 2.0.

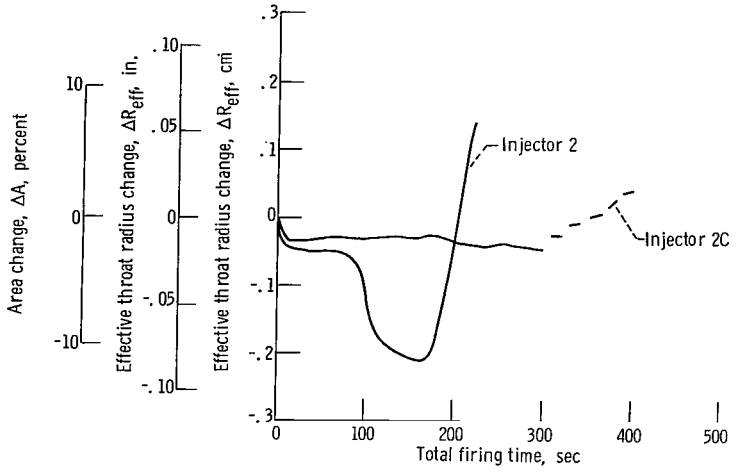

(a) Erosion results of zirconia insert (cast, mixed grain) with injector 2C.

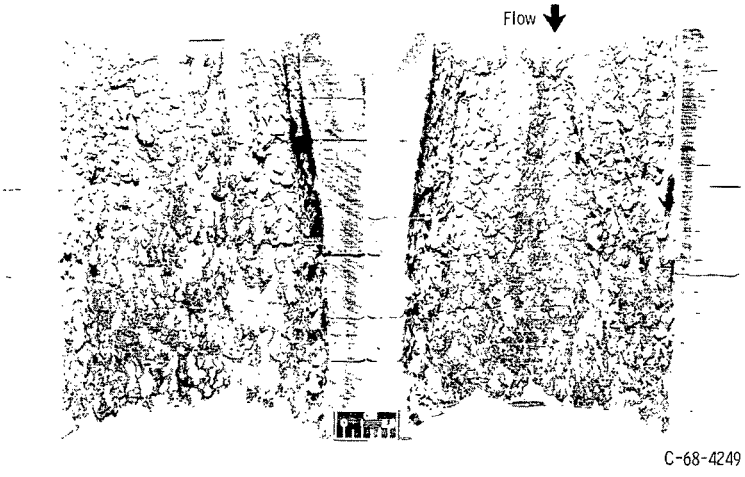

(b) Injector 2. Silica phenolic chamber section after 433-second total firing time; chamber pressure, 690 kN/m^2 (100 psia); oxidant-to-fuel mixture ratio, 2.0.

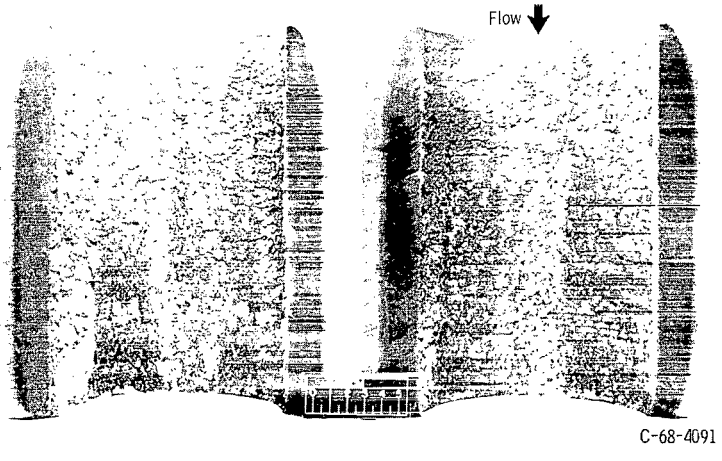

(c) Injector 2C. Silica phenolic chamber section after 428-second total firing time; chamber pressure, 690 kN/m^2 (100 psia); oxidant-to-fuel mixture ratio, 2.0.

Figure 33. - Ablative and throat insert erosion comparison - injectors 2 and 2C.

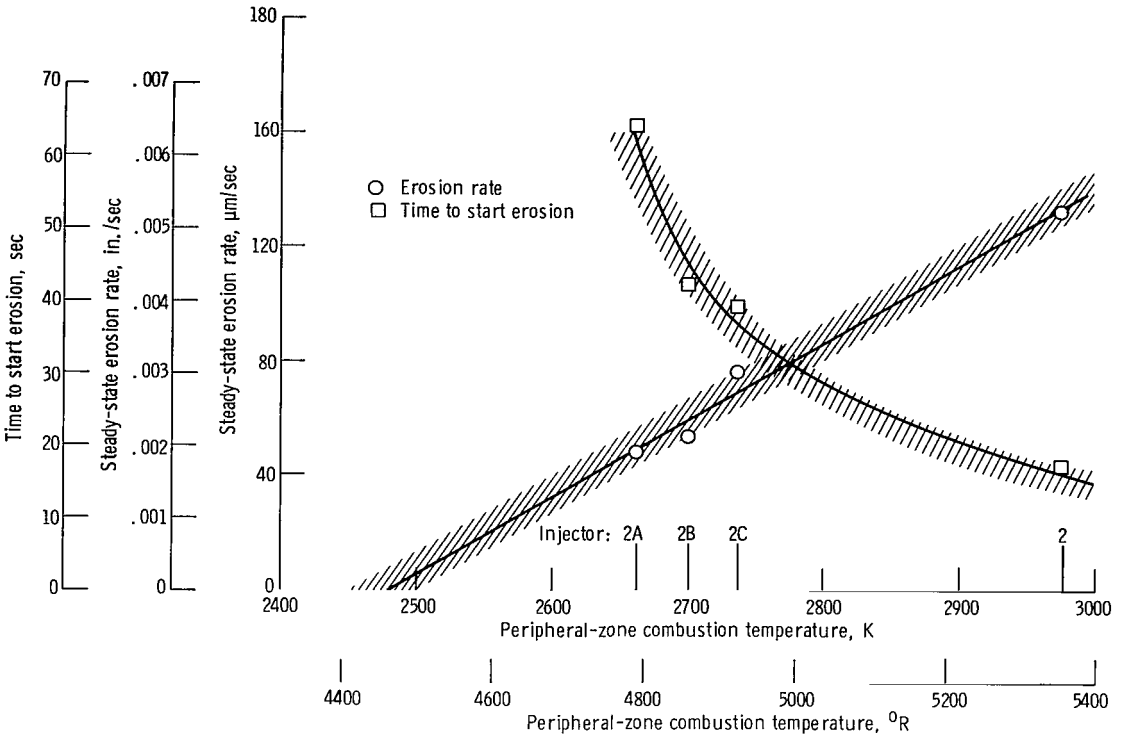

Figure 34. - Effect of peripheral-zone combustion temperature on ablative throat erosion. (See table II.)

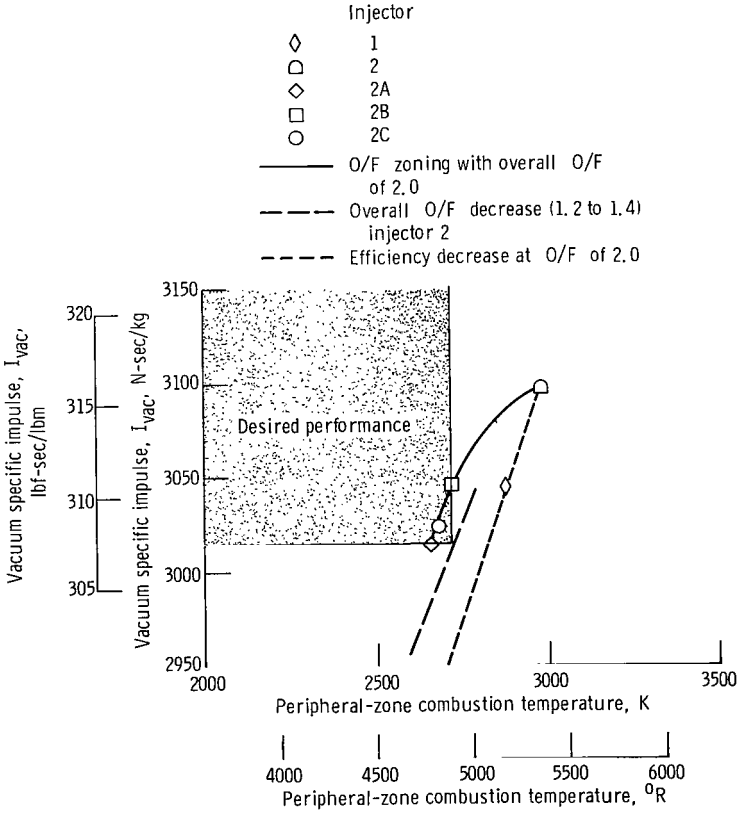

Figure 35. - Effect of O/F zoning on peripheral-zone combustion temperature and performance. Overall mixture ratio, 2.0.

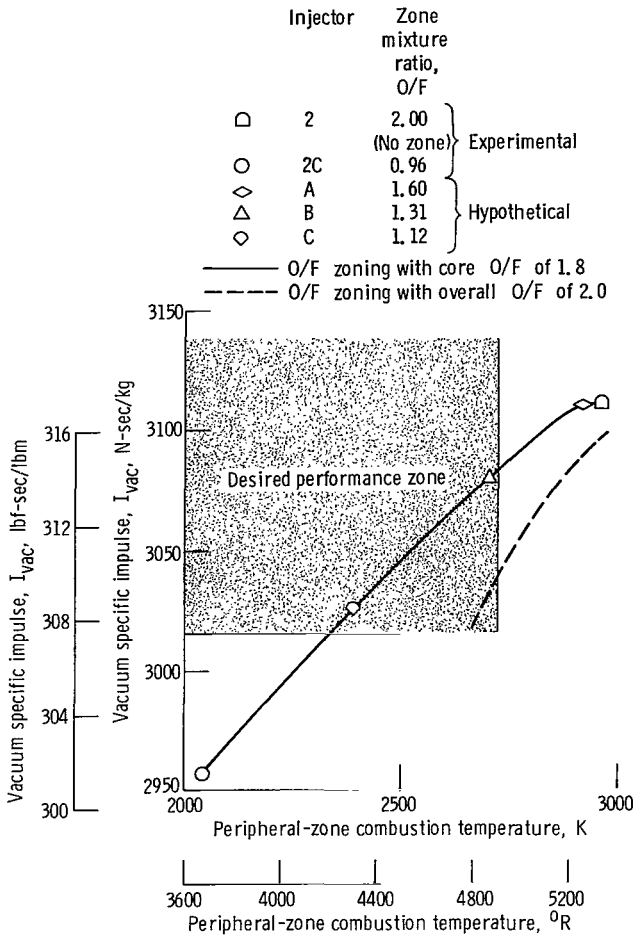

Figure 36. - Effect of O/F zoning on peripheral-zone combustion temperature and performance. Core mixture ratio, 1.8.

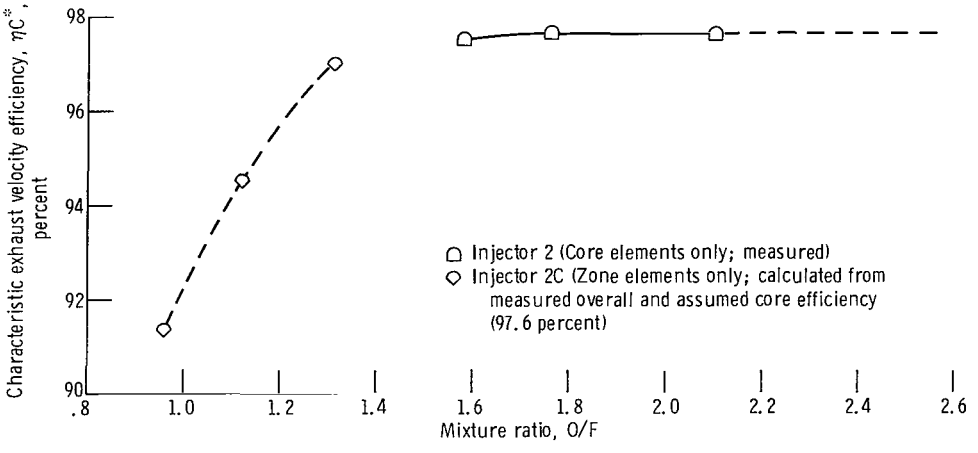

Figure 37. - Zone and core element characteristic exhaust velocity efficiency.

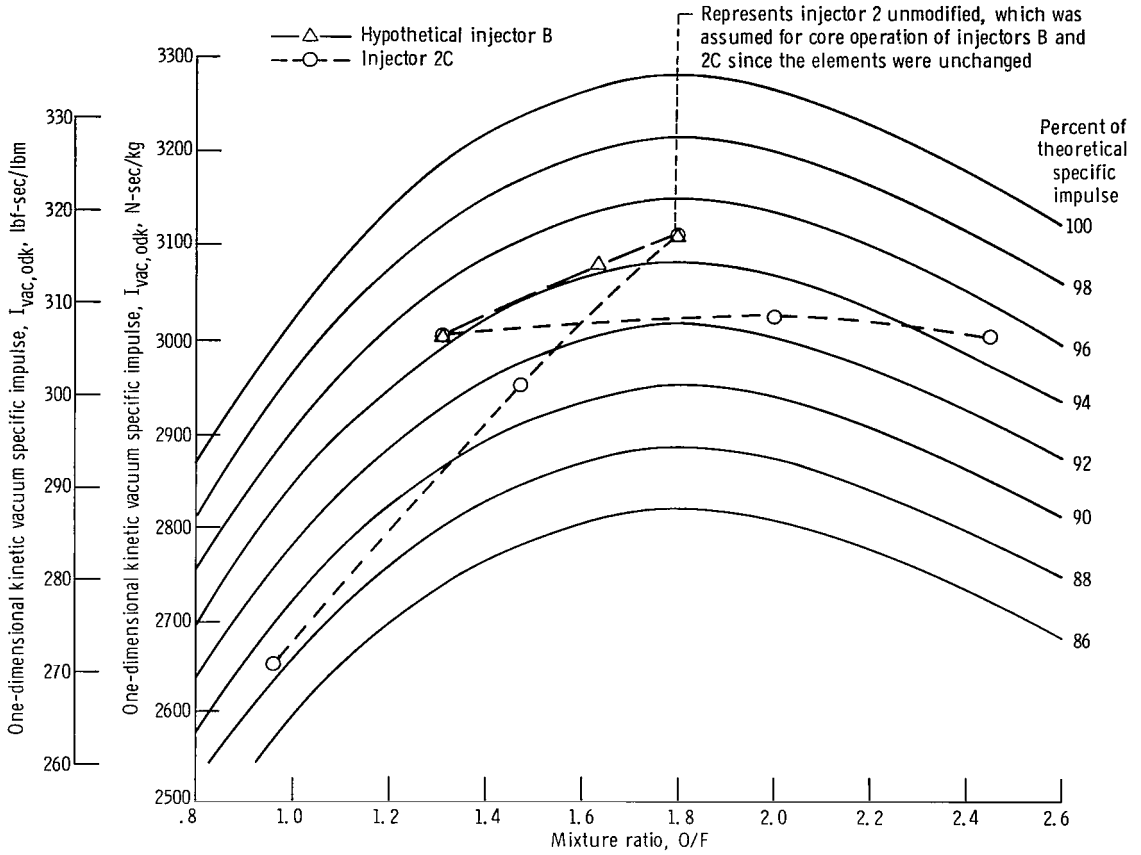

Figure 38. - Calculated engine performance for nozzle expansion area ratio of 60.

"The aeronautical and space activities of the United States shall be conducted so as to contribute . . . to the expansion of human knowledge of phenomena in the atmosphere and space. The Administration shall provide for the widest practicable and appropriate dissemination of information concerning its activities and the results thereof."

— NATIONAL AERONAUTICS AND SPACE ACT OF 1958

NASA SCIENTIFIC AND TECHNICAL PUBLICATIONS

TECHNICAL REPORTS: Scientific and technical information considered important, complete, and a lasting contribution to existing knowledge.

TECHNICAL NOTES: Information less broad in scope but nevertheless of importance as a contribution to existing knowledge.

TECHNICAL MEMORANDUMS: Information receiving limited distribution because of preliminary data, security classification, or other reasons.

CONTRACTOR REPORTS: Scientific and technical information generated under a NASA contract or grant and considered an important contribution to existing knowledge.

TECHNICAL TRANSLATIONS: Information published in a foreign language considered to merit NASA distribution in English.

SPECIAL PUBLICATIONS: Information derived from or of value to NASA activities. Publications include conference proceedings, monographs, data compilations, handbooks, sourcebooks, and special bibliographies.

TECHNOLOGY UTILIZATION PUBLICATIONS: Information on technology used by NASA that may be of particular interest in commercial and other non-aerospace applications. Publications include Tech Briefs, Technology Utilization Reports and Technology Surveys.

Details on the availability of these publications may be obtained from:

SCIENTIFIC AND TECHNICAL INFORMATION OFFICE

NATIONAL AERONAUTICS AND SPACE ADMINISTRATION

Washington, D.C. 20546